

A Comprehensive Review on the Characteristics and Modeling of Lithium-Ion Battery Aging

Wiljan Vermeer^{ID}, Student Member, IEEE, Gautham Ram Chandra Mouli^{ID}, Member, IEEE,
and Pavol Bauer^{ID}, Senior Member, IEEE

Abstract—Battery aging is one of the critical problems to be tackled in battery research, as it limits the power and energy capacity during the battery's life. Therefore, optimizing the design of battery systems requires a good understanding of aging behavior. Due to their simplicity, empirical and semiempirical models (EMs) are frequently used in smart charging studies, feasibility studies, and cost analyses studies, among other uses. Unfortunately, these models are prone to significant estimation errors without appropriate knowledge of their inherent limitations and the interdependence between stress factors. This article presents a review of empirical and semiempirical modeling techniques and aging studies, focusing on the trends observed between different studies and highlighting the limitations and challenges of the various models. First, we summarize the main aging mechanisms in lithium-ion batteries. Next, empirical modeling techniques are reviewed, followed by the current challenges and future trends, and a conclusion. Our results indicate that the effect of stress factors is easily oversimplified, and their correlations are often not taken into account. The provided knowledge in this article can be used to evaluate the limitations of aging models and improve their accuracy for various applications.

Index Terms—Aging, battery, degradation, lithium, modeling.

I. INTRODUCTION

SINCE they were first commercialized by Sony in 1991 [1], lithium-ion battery (LIB) technology has been widely adopted due to its relatively high energy and power density, high efficiency, and rather a long lifetime [2]. Today, LIBs play a vital role in the energy transition; they help integrate renewable energy sources (RESs), provide ancillary services, and reduce transportation emissions. In addition, LIBs are also widely used in the mobile device industry, aerospace and aviation industry, and defense industry [3], [4]. All of these contribute to a rapidly increasing LIB market. However, despite its growing market and relatively good performance, climate change and particularly electric vehicle (EV) applications push for lower costs and higher energy densities over a long lifetime. Unfortunately, these metrics are generally trade-offs, and therefore, understanding battery aging and modeling is critical for optimizing LIB performance.

This article presents a review of empirical and semiempirical modeling techniques and aging studies, focusing on the

Manuscript received August 10, 2021; revised November 4, 2021; accepted December 10, 2021. Date of publication December 23, 2021; date of current version April 20, 2022. This work was supported by TKI Urban Energy. (*Corresponding author: Wiljan Vermeer.*)

The authors are with the Department of DC Systems, Energy Conversion & Systems, Delft University of Technology, 2628 CD Delft, The Netherlands (e-mail: w.w.m.vermeer@tudelft.nl).

Digital Object Identifier 10.1109/TTE.2021.3138357

TABLE I
COMPARISON OF DIFFERENT AGING MODEL TECHNIQUES

Model	Complexity	Accuracy	Amount of data	Applications
PBM	high	high	low	battery design
ECM	medium	medium	high	SoH estimation
MLM	medium-high	medium	high	SoH estimation
EM	low	low-medium	high	System design & Optimization

trends observed between different studies and highlighting the limitations and challenges of the various models.

A. Battery Aging Modeling

Methods for modeling LIB degradation behavior are divided into four different categories: 1) physics-based models (PBMs); 2) equivalent circuit models (ECMs); 3) machine learning models (MLMs); and 4) empirical and semi-empirical models (EM). A comparison of these models is given in Table I. PBMs, also known as electrochemical models, intended to model the electrochemical and physical processes in the battery. The first PBM was developed by Doyle *et al.* [5] and was based on the porous electrode model [6]. The pseudo-2-D model is expanded on this by adding a thermal model [7], including diffusion kinetics and Butler–Volmer kinetics [6]. Later, the effect of parasitic side reactions, such as solvent oxidation [8] or SEI layer growth [9], [10], was added to these equations to account for degradation. Others have tried to reduce the computational complexity for these models to be more widely applicable [11]. PBMs can achieve high accuracy, but they require many partial differential equations and a thorough understanding of all physical and chemical mechanisms. Furthermore, LIB aging is frequently caused by multiple factors, making molecular modeling even more difficult and prone to miss out on macrolevel effects [12]. As a result, electrochemical models are generally not used by nonchemical engineers/researchers [13].

ECMs do not require this information and instead model the transient response of the battery using passive circuit components, such as resistances, capacitances, and inductances. More complex models can also be used to simulate the internal diffusion and charge transfer processes. Based on impedance data, aging can be incorporated using variable components. This, however, requires large test matrices to quantify the aging with respect to operational conditions. Due to their mathematical simplicity, they are frequently used in real-time applications, such as battery state estimations [14]. Often

combined with state estimators, such as Kalman or particle filters [12], [14].

Another common state-of-charge (SoC) and state-of-health (SoH) estimation technique involves machine learning (ML), such as support vector machine or neural networks. Different ML approaches exist; some train the algorithm to extract the SoH from the differential voltage curve or incremental capacity curve of the battery [15], [16]. The advantage of these approaches is that they only require easily obtained parameters, such as voltage, current, and temperature. Others combine ML with different models to train the algorithm based on model parameters, such as ohmic resistance, polarization resistance, and polarization capacitance [17], [18], or combine empirical modeling techniques with regression models to predict the SoH [19]. High accuracies can be obtained with ML methods; however, large datasets are needed to train the algorithms [12], [20]. Finally, empirical and semi-EMs curve-fit the relationship of various stress factors onto the data resulting in a relatively simple analytical formula. Their simplicity allows using EMs in a wide variety of studies, such as system-level design problems, optimization models, and battery management systems, among other things. In addition, the analytical formulas give an intuitive feel to the effect of various stress factors. However, large test matrices are required to decouple their impact (if even possible), which is generally limited by the available equipment. As a result, EMs are prone to oversimplify the complex behavior of LIB aging and the correlation between stress factors; this is discussed in more detail in Section I-B.

B. Challenges of Empirical and Semiempirical Aging Models

Without a good understanding of LIB aging behavior and modeling limitations, the simplicity of EMs can pose challenges as they can easily lead to significant modeling errors. A summary of these challenges is given in the following.

- 1) *Accelerated Test Conditions:* Aging tests are frequently performed under accelerated aging conditions, such as high temperature, high C-rates, and high voltages to speed up aging. While this reduces the amount of time required for testing, it also reduces the accuracy of the models when they are utilized outside of the test conditions. For example, models are often developed based on temperatures of 40 °C and higher, whereas very rarely models are tested below 25 °C, and even fewer studies have evaluated multiple operating conditions below 25 °C. As will be demonstrated in this study in Section III-4, the use of testing conditions at temperatures that will never actually be reached or sustained for longer periods of time during normal operation can cause unreliable results, especially at temperatures below room temperatures, where the effect of high-temperature aging mechanisms will decrease, and other aging mechanisms take over.
- 2) *Limited Test Conditions:* Large test matrices are required to accurately model the effect of multiple stress factors, which are generally limited by the amount of available equipment. Here, a good understanding of the expected

aging behavior can help to determine the test conditions more strategically.

- 3) *Stress Factor Interdependence:* A good understanding of the interdependencies between stress factors is required to select an appropriate model and testing conditions for a particular use case. For example, based on the reviewed studies in this article, it is observed that a strong correlation between the effect of temperature and C-rate exists. However, not many models model the interdependency of these stress factors. As a result, the actual operating range of the model might be limited to only the accelerated testing conditions. Furthermore, even within the test condition range, significant errors might occur when these interdependencies are not considered.
- 4) *Modeling Limitations:* Besides the effect of operational conditions, a good understanding of the model's fundamental limitations is also required. For example, depending on the chosen parametrical fit, EMs might be limited to a specific part of the battery lifetime or might be less suited for applications with very irregular charge cycles or applications with a different calendar-to-cyclic aging ratio.

The goal of this article is to mitigate the effects of the abovementioned challenges and limitations by providing a comprehensive review of empirical and semiempirical LIB aging models, as well as the accompanied aging behavior.

C. Related Work and Scientific Gap

In [21] and [22], an in-depth review of the main aging mechanisms on a material level is discussed. These studies are elaborated in [23] and [24], where the authors also review the factors influencing aging on a cell and battery pack level. Jafari *et al.* [6], Barré *et al.* [12], and Scarfogliero *et al.* [25] review the main aging mechanisms and provide an overview of different aging estimation techniques, including electrochemical models, ECMS, EMs, and statistical models. A similar approach for data-driven health diagnostics and prognostic techniques is performed in [20]. In [26], a comparison of several EMs is performed based on a conceptual smart grid framework. Furthermore, several studies have reviewed the various techniques for SoH estimation [27]–[30]. Lucu *et al.* [29] discuss different types of self-adaptive SOH monitoring techniques, such as support vector regression, neural networks, or particle filter method. In addition, a more broad overview of different types of SOH and remaining-useful-life (RUL) estimation techniques is given in [27], [28], and [30], including direct measurement techniques, model-based techniques, and adaptive filtering techniques.

All of the papers mentioned above aim at providing a broad overview of different kinds of aging mechanisms or aging estimation techniques, whether model-based techniques and data-driven techniques are self-adaptive techniques. In most of them, EMs are briefly mentioned as a part of this. However, given the scope of these papers, they do not provide an in-depth review of different EMs nor do they provide any

insights into the correlations found between different studies. Even [26], which is entirely focused on EMs, provides a simplified description of the effect of operational stress factors. Furthermore, none of the abovementioned papers actually reviews and compares the aging behavior of different aging studies, which makes it even more difficult to provide generalizations in terms of the impact of operational conditions or modeling accuracy. As explained above, this is especially problematic for EMs since, without a proper understanding of battery aging, empirical aging modeling, and its limitations and challenges, the simplicity of EMs can easily lead to significant modeling errors in a wide variety of studies.

D. Contribution

LIB degradation is an important factor for developing new LIBs and optimizing their technoeconomic performance. In this regard, multiple studies have reviewed the various methodologies for aging estimation. However, based on the aforementioned challenges and related work, it is concluded that a significant scientific gap still exists since no study has yet thoroughly reviewed empirical and semi-EMs, and has investigated the correlations between different studies to highlight the limitations of the models and focus on the reasons for the observed trends and insights. Due to the simplicity and widespread use of EMs, this can potentially result in significant modeling errors. To this extent, the main contributions of this study are summarized as follows:

- 1) a comprehensive review of empirical and semiempirical modeling techniques for LIB aging, with a focus on operational stress factors and their interdependence, modeling techniques, limitations, and challenges, so that these models can be used accurately at the relevant operating conditions;
- 2) a detailed review of the aging behavior of various LIB cells, investigating the correlations between different aging studies and examining the relationship with operating conditions, aging mechanisms, and modeling techniques.

E. Organization

The remainder of this article is organized as follows. Section II summarizes the main aging mechanisms for LIBs. Next, the review of aging behavior and different modeling techniques is discussed in Section III. Here, a distinction is made between calendar aging and cyclic aging. The modeling techniques, limitations and challenges, and key insights are discussed per stress factor for both calendar aging and cyclic aging. Therefore, the structure of Section III is given as follows:

- 1) calendar/cyclic aging;
 - a) stress factor X;
 - i) modeling techniques;
 - ii) modeling limitations and challenges;
 - iii) key insights.

Next, the current challenges and future trends regarding LIB aging and aging modeling are described in Section IV. Finally, the conclusion is presented in Section V.

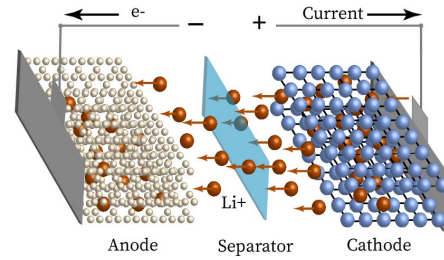


Fig. 1. Simplified representation of an LIB consisting of an anode, cathode, separator, and electrolyte (the electrolyte is not shown for clarity, as it fills the entire battery). The arrows indicate a charging process where the Li-ions intercalate into the anode, resulting in an opposite electron flow.

II. MAIN AGING MECHANISMS

Fig. 1 shows a simplified representation of an electrochemical battery. The four main components of an LIB are given as follows.

- 1) Anode, the most often used material is graphite [12], [21], [31]; other common materials are lithium–titane–oxide (LTO) or silicon [32].
- 2) Cathode, which is made of a composition material that contains lithium. Commonly used materials are lithium–iron–phosphate (LFP), lithium–nickel–manganese–cobalt (NMC) oxide, lithium–manganese oxide (LMO), and lithium–nickel–cobalt–aluminum (NCA).
- 3) Electrolyte, a composition of lithium salts and organic solvents [26]. The electrolyte is mainly used to transfer ions between the cathode and the anode.
- 4) Separator, a porous plastic that separates the anode and the cathode to prevent short-circuiting the electrodes.

During charging, Li-ions deintercalate¹ from the cathode and move through the electrolyte and separator before they intercalate at the anode. The resulting flow of ions creates an electrical current opposite to the flow of electrons, as shown in Fig. 1. The degradation of LIBs occurs during both cycling and idle states, and is caused by physical stress and chemical side reactions [2], [23]. In addition, many factors influence battery degradation, such as cell chemistry, cell design, pack design, and operating conditions. LIB aging is commonly categorized into three different aging modes [21], [23], [31], [33], [34].

- 1) *Loss of Lithium Inventory (LLI)*: It represents the loss of active lithium ions that are no longer available for cycling. Causes for LLI can be parasitic side reactions, such as surface film formation, decomposition reactions, and lithium plating, among other things. LLI is associated with capacity fade, i.e., the loss of effective mAh of the cell.
- 2) *Loss of Active Material (LAM)*: It represents the loss or structural degradation of the available anode or cathode material. Possible causes include electrode surface layer growth or cycling-induced cracks/exfoliation. LAM can cause both power and capacity to fade.
- 3) *Conductivity Loss (CL)*: It, also known as contact loss [21], describes the degradation of electrical parts,

¹Intercalation is the insertion of molecules into the electrodes.

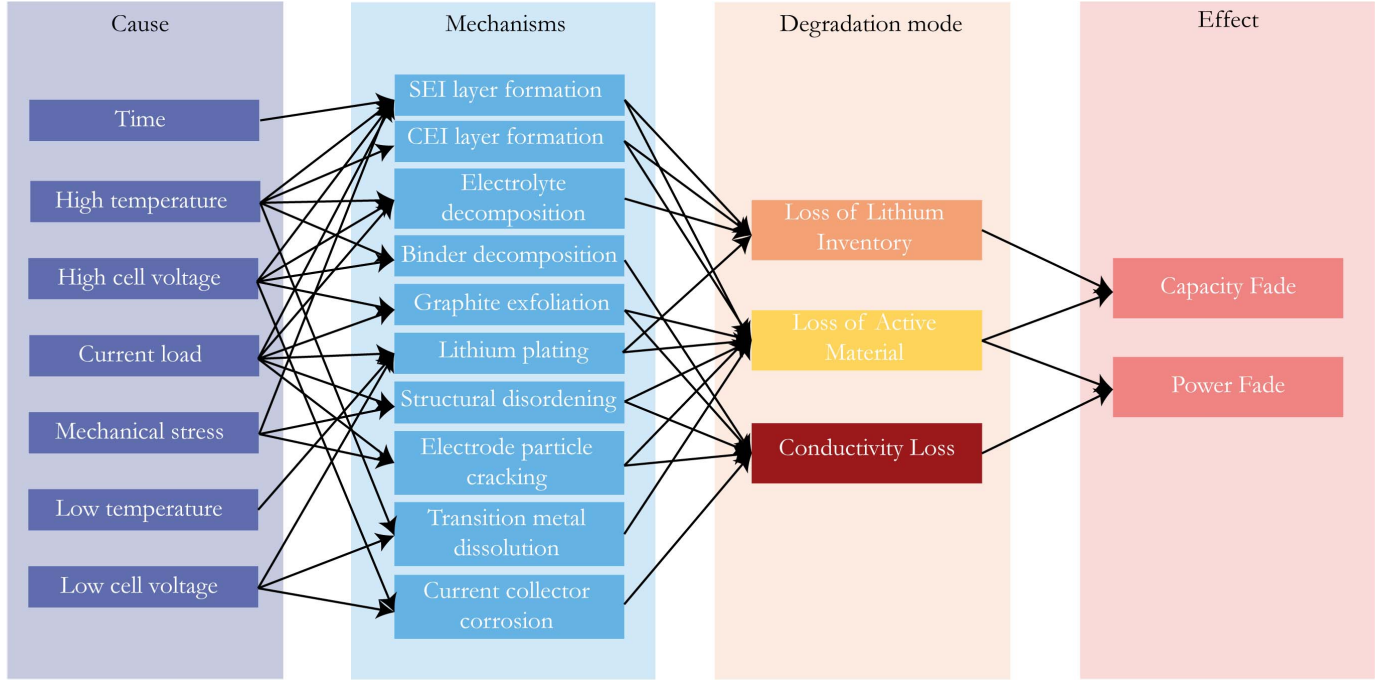


Fig. 2. Overview of the correlation between operational stress factors (the causes for degradation), the corresponding aging mechanisms, aging mode, and their effect on LIB aging. Based on a combination of [2], [31], and [33].

such as the current collector corrosion and binder decomposition.

The fourth addition could be the loss of electrolytes, which would lead to LAM and CL after a certain point, and is, therefore, not separately mentioned. Even though differentiated into three categories, the degradation modes often interact, and a single degradation mechanism, such as surface layer formation, can trigger multiple degradation modes. A summary of operational conditions, the corresponding aging mechanisms, and their effect on LIB aging is shown in Fig. 2. Furthermore, a graphical representation of all aging mechanisms is shown in Fig. 3. Sections II-A and II-B will discuss these aging mechanisms; here, a division is made between the mechanisms that occur at the anode and the cathode, respectively. The aging of the electrolyte and its effect on battery aging mainly takes place at the electrodes [21] and is, therefore, not separately discussed.

A. Anode Aging

The majority of LIBs use graphite as their anode material [21], [25], [35], so this section focuses on graphite-based LIBs.

1) *Solid Electrolyte Interphase Layer:* The operating voltages of various common electrode materials in comparison to the electrochemical stability window of organic electrolytes are shown in Fig. 4. The operating voltage of graphite anodes is in the 0.05 V–1 V range [2], [36], which is outside the organic electrolyte stability window of 1–4.5 V. As a result, graphite-based LIBs are thermodynamically unstable, resulting in a reductive electrolyte decomposition reaction. This reaction consumes Li⁺ ions and forms a surface layer on the anode,

resulting in LLI and LAM [2], [12], [21]. Especially in the first few cycles, the reaction rate is high, creating a surface layer permeable for Li-ions but less permeable for electrolyte components. This reduces the rate of decomposition and further electrode corrosion [21], [37]–[39]. However, even though the reaction rate reduces, the transport of solvated lithium and other electrolyte components through this semipermeable layer continues throughout the battery's life. This reaction mainly occurs at the interphase between the electrolyte and the anode and is called the solid electrolyte interphase (SEI) layer.

The SEI layer's growth is often one of the main aging factors of graphite anodes. It reduces the battery's available energy capacity and power handling capability. Another type of anode surface layer grows on the basal plane surface and is impermeable for Li-ions and, therefore, sometimes referred to as the non-SEI layer [41]. However, often the SEI and non-SEI layers are both referred to as SEI layer [21]. Therefore, this convention is followed here as well.

After the initial formation of the SEI, it continues to grow during both cycling and idle conditions. The rate at which the SEI layer grows is dependent on the operating conditions of the cell [42], [43]. During idle conditions, SEI growth is mainly driven by temperature and SoC. At a higher SoC, more Li-ions are intercalated into the anode, decreasing the anode potential and increasing the reductive reaction rate [36]. In addition, an increasing temperature also increases the reaction rate and might cause the less stable organic SEI components to change into more stable inorganic products, reducing the SEI layer's ionic conductivity. At extreme temperatures above 60 °C, even thermal runaway can cause the cell to catch fire or explode. Aside from SoC and temperature, volume changes caused by the (de)intercalation

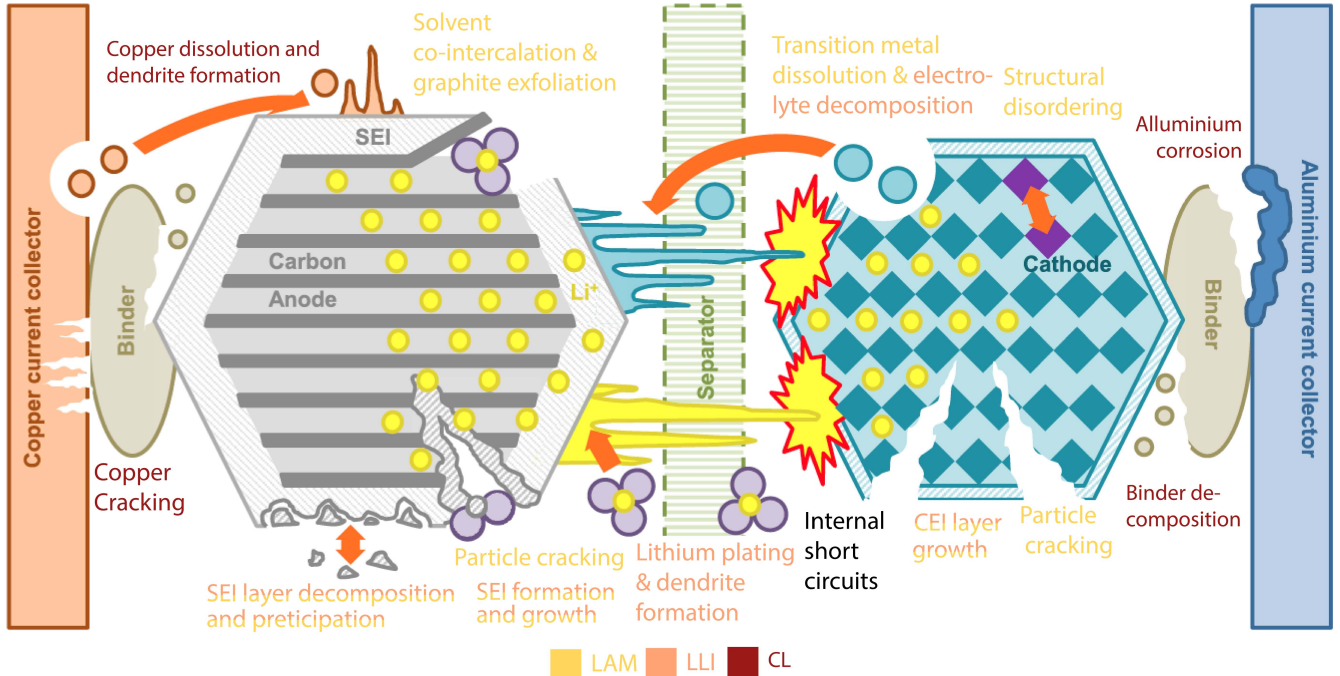


Fig. 3. Graphical summary of aging mechanisms in graphite-based LIBs. The aging mechanisms are color coded with respect to the accompanied degradation mode. The figure is adapted from material made publicly available by Birki *et al.* [31], under Creative Commons Attribution 4.0 License CC-BY.

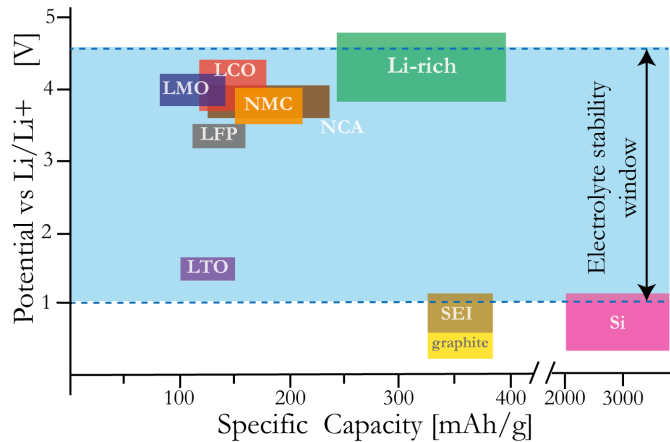


Fig. 4. Voltage versus energy capacity of five common electrode materials compared to the electrochemical stability window of liquid organic electrolytes, adapted from [24] and [40]. It shows that graphite is outside the electrochemical stability window of organic electrolytes, rendering graphite-based Li-ion batteries thermodynamically unstable and causing SEI layer growth.

of Li-ions during cycling cause mechanical stress on the electrodes. These volume changes can crack the SEI, allowing new reactions to occur. As a result of this crack and repair, the SEI continues to grow, resulting in additional LLI and LAM [21], [44], [45]. Furthermore, cycling, especially with high C-rates, creates a more porous SEI layer compared to idle conditions [42], [43]. This increased porosity allows for more reductive reactions to occur, whereas a denser SEI layer reduces the reaction rate. Other factors influencing the reaction rate are electrolyte composition and electrode balance [39], [46].

Two opposing theories exist regarding SEI formation: 1) the first theory assumes that the formation takes place at the electrode/electrolyte interface and that the electronic conductivity of the SEI should be the limiting factor of formation [22] and 2) the second theory states that SEI formation takes place at the anode–SEI interface and is limited by the solvent diffusion process [47]. However, both theories result in an aging behavior that follows a $\sqrt{\text{time}}$ relationship, which is typical for the passivation character of the SEI layer and similar to what is often observed in experiments.

2) *Lithium Plating:* At lower temperatures, generally below 20 °C, the diffusion rate of lithium into the anode or electrolyte reduces, and the intercalation potential of graphite material approaches that of metallic lithium. Metallic lithium plating may occur as a result of this. Lithium plating is especially likely to occur at low SoC, low temperature, and high C-rates [31]. Furthermore, after a certain age, the anode resistance can reach a critical limit. After this limit, the anode potential drops below 0 V versus Li/Li+, and lithium plating starts to occur [43], [48].

Unlike SEI layer growth, lithium plating is a positive reinforcing phenomenon: as it occurs, it deposits on the anode, reducing the active surface area, resulting in a higher current density at the remaining available pores, and further increasing the metal plating. As a result, a knee point in the degradation behavior is frequently observed at the age at which lithium plating occurs. An example of this is shown in Fig. 5(a) and (b), where two inflection points are observed in both the capacity and impedance deterioration. Lithium plating causes LLI and possibly reduces the cell's safety, as lithium dendrites can start to grow, leading to internal short circuits [21].

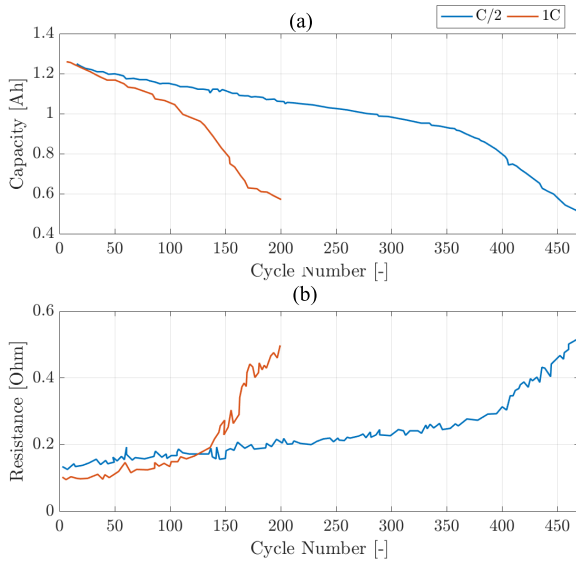


Fig. 5. Effect of lithium plating on remaining (a) capacity and (b) internal resistance for two LCO cells: after a certain age, lithium plating can start to occur, causing an increased degradation rate (inflection point) in both capacity and resistance deterioration [22].

3) *Mechanical Stress at Anode*: The intercalation of lithium ions into the anode can result in abrupt changes in volume as the particles undergo a phase transition [21], [49]. During a phase transition, the orientation of the molecules changes as more lithium is inserted, resulting in different geometrical and electrical properties. This causes volume change-induced mechanical stress, which can lead to anode structural damage (LAM), surface layer cracking (LLI and LAM), and contact loss with the composite electrode (CL). The active material's volume change may also result in a decrease in electrode porosity, which is required for the electrolyte to reach the bulk of the electrode [21].

4) *Transition Metal Dissolution*: Most lithium batteries' cathodes contain transition metals, such as iron, nickel, cobalt, manganese, and vanadium. Similarly, most battery electrolytes contain the salt LiPF_6 . The cycling and storage of these cells, particularly at high cell voltages and high temperatures [50], can result in the formation of hydrogen fluoride (HF) from impurities inside the electrolyte, which increases the acidity of the electrolyte. The resulting HF corrodes the cathode and dissolves the transition metals, contributing to several degradational mechanisms in both the anode and the cathode, causing capacity fade and impedance rise. To begin, metal dissolution can cause structural degradation of the cathode (LAM), resulting in reduced lithium insertion capability [51]. Furthermore, after dissolution, the metals can migrate through the electrolyte and deposit on the anode, acting as catalysts for the reductive decomposition reaction that causes SEI layer growth [52]. Finally, the deposition of transition metals on the anode during this reductive process may induce the formation of lithium metal dendrites on the deposited metals (LLI and LAM). These dendrites can cause internal short circuits, posing a significant safety risk.

Particularly, spinel-containing chemistries, such as LiMn_2O_4 , are vulnerable to transition metal dissolution,

as the extent of dissolution can be much greater, resulting in more structural degradation of the cathode (LAM). Although transition metal dissolution is unavoidable during the charging process, it can be reduced by reducing impurities in the electrolyte, using dopants, and using protective coatings around the cathode to reduce direct contact between the cathode and the electrolyte [52].

5) *Other Aging Mechanisms*: Other degradation mechanisms at the anode include graphite exfoliation: the structural degradation of graphite (LAM) as a result of high current densities or solvent co-intercalation, particle cracking (LAM) as a result of mechanical stress or high current load, binder decomposition (CL) caused by high temperatures and high cell voltages, corrosion of current collectors (CL), and loss of electrical contact (CL). For more details, interested readers are direct to [21], [31], and [22].

6) *Lithium–Titanate Oxide and Silicon-Based Anodes*: The main advantage of LTO anodes over graphite anodes is their higher potential, as shown in Fig. 4. As a result, these anodes are not thermodynamically unstable and, therefore, do not form an SEI layer [53]. Furthermore, LTO is a zero-strain material that does not change volume when charged or discharged. As a result, LTO-anode batteries can handle extremely high C-rates while still retaining a long lifetime. This comes at the cost of a lower energy density due to their higher potential [54].

On the other hand, silicon (Si)-based anodes have a superior energy density, with a theoretical capacity of 3580 mAh/g, compared to 350 mAh/g for graphite-based anodes and 175 mAh/g for LTO-based anodes [55]. However, during cycling, the volume of the silicon particles can change by up to 280%. These volume changes cause excessive mechanical stress, reducing their lifetime significantly [32].

B. Cathode Aging

The cathode is the lithium-containing part of a cell, and the limiting factor during charging as its maximum voltage determines the end of charge voltage. Similarly, the anode is the limiting factor during discharge due to its minimum discharge voltage limit [31], [56]. In terms of aging, the cathode is generally regarded as less significant [57], [58].

Common cathode chemistries are LCO, LFP, NMC, LMO, and NCA. These chemistries all have their strengths and weaknesses, varying in energy and power density, toxicity, safety, cost, and natural abundance, among other things. Although many more chemistries exist, this review focuses on the most common materials.

The main aging mechanisms of cathode materials include surface film formation, mechanical stress, and transition metal dissolution. Other aging mechanisms on the inactive components include current collector corrosion, binder decomposition, and conducting agent oxidation [21], [49], as shown in Fig. 3. The most significant aging mechanisms are discussed in the following.

1) *Cathode Surface Layer Film*: Surface layer films (also known as cathode electrolyte interphase (CEI) layer) can form on the cathode, similar to the anode, but due to

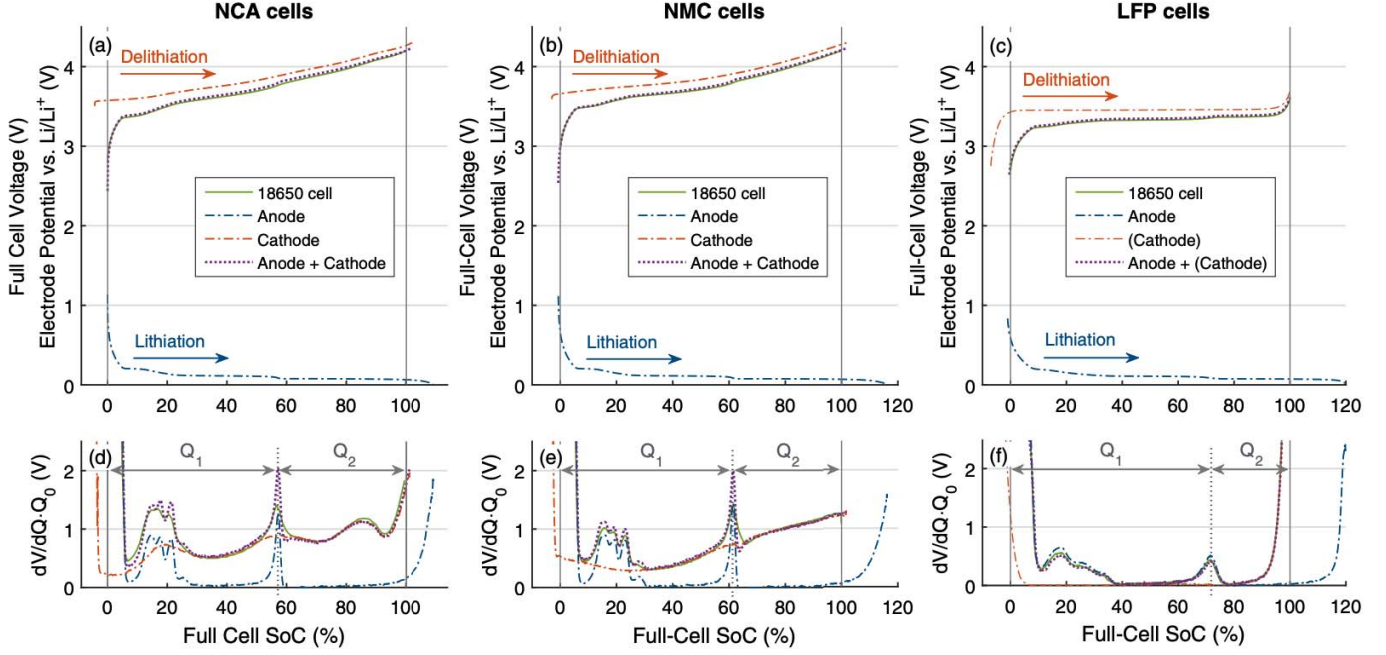


Fig. 6. Voltage and differential voltage profile of (a) NCA, (b) NMC, and (c) LFP full cells during low current charging, including a reconstructing of full cell voltage based on half-cell voltage profiles (dotted lines). (d)–(f) Differential voltage spectra of the three different cells. (c) and (f) Cathode voltage profile of an LFP cell is very flat compared to the other two chemistries due to the two-phase regime. The figure is obtained from the publicly available material of Han *et al.* [23], under the Creative Commons Attribution 4.0 License CC-BY.

electrolyte oxidation and salt deposition [21], [59], [60]. In contrast to the SEI layer, the cathode surface layer shows low lithium-ion conductivity, increasing the impedance. Furthermore, also, gas evolution is possible [21], [22]. According to Broussely *et al.* [22], organic products formed by reduction at the anode may also be transported to the cathode, where they are oxidized and deposited on the cathode surface, resulting in LAM and LLI. Similar findings have been made in [61]. Unfortunately, due to the higher voltage of the cathode, this surface film layer is more difficult to detect [59], [60].

2) *Mechanical Stress at Cathode*: The cathode, like the anode, can go through phase transitions during the intercalation and deintercalation of Li-ions, which can result in LAM and CL. The amount of volume change varies depending on the chemistry. LFP cells, for example, only have a two-phase regime consisting of FePO₄ and LiFePO₄ [62]. As a result, the (cathode) voltage and differential voltage profiles of these cells are very flat, as shown in Fig. 6. Because of this two-phase regime, LFP cells exhibit only a slight increase in volume, around 6.8% [1], and have a very high rate capability and a good lifetime [62]. Other chemistries, such as NCA or NMC, show multiple phase transitions in both cathode and anode voltage profiles. Manganese-containing chemistries, particularly LMO, exhibit additional mechanical stress as a result of the Jahn-Teller distortion of Mn³⁺ particles. This results in a phase change from cubic to a tetragonal form. In the case of LMO, this can increase the cathode volume by approximately 16% [2], [21], resulting in additional LAM [63], [64]. The Jahn-Teller distortion occurs at low SoC. By controlling the end-of-discharge voltage (EODV) and adding dopants, the capacity fade caused by volume change can be reduced.

3) *Transition Metal Dissolution*: As mentioned above, transition metals in the cathode can dissolve resulting in structural degradation of the cathode (LAM).

III. REVIEW OF EMPIRICAL DEGRADATION MODELING

This section discusses the most common empirical and semiempirical modeling techniques and their limitations. Furthermore, the cells' aging behavior is discussed and, where possible, explained using the described degradation mechanisms. LIB degradation can be divided into two different types.

- 1) *Calendar Aging*: The aging that occurs when the cell is in an idle state. Calendar aging results from side reactions that take place due to thermodynamic instability of the materials [22].
- 2) *Cyclic Aging*: It includes the aging as a result of cycling the battery. Various kinetically induced effects, such as volume variations or concentration gradients, result in additional degradation [22], [36].

Following the reviewed studies, this article focuses more on capacity fading than a resistance increase. A summary of all studies and their testing conditions can be found in Tables II and III.

A. Calendar Aging

Capacity fading due to calendar aging can be separated into two parts: reversible and irreversible capacity loss. By recharging the battery, the reversible part can be restored, whereas the irreversible part cannot. This review focuses on the irreversible part of calendar aging. Reversible capacity loss is studied in more detail in [65] and [66]. The three factors that influence calendar aging are: 1) temperature; 2) SoC; and 3) time.

TABLE II
OVERVIEW OF STUDIES INVESTIGATING EMPIRICAL AND SEMIEMPIRICAL CALENDAR LIFE MODELS

Study	Chemistry	Capacity	Resistance	Factors	Conditions		
					Temp.	SoC	Time
[72]	LFP	✓	x	SoC, T, time	30-60 °C	30-100%	850 days
[73]	LFP	✓	x	SoC, T, time	40-55 °C	10-90%	800 days
[74]	LFP	✓	✓	SoC, T, time	30-60 °C	30-100%	450 days
[75]	LFP	✓	x	SoC, T, time	30-50 °C	30-90%	300 days
[63]	LFP	✓	✓	SoC, T, time	30-60 °C	30-100%	225 days
[76]	LFP	✓	✓	SoC, T, time	25-55 °C	30-100%	305 days
[77]	LFP	x	✓	SoC, T, time	40-55 °C	10-90%	225 days
[78]	LFP	✓	x	SoC, T, time	40-60 °C	40-80%	105 days
[79]	LFP	✓	x	SoC, T, time	40-55 °C	10-90%	-
[80]	NMC	✓	✓	SoC, T, time	30-60 °C	30-100%	480 days
[81]	NMC-LMO	✓	x	SoC, T, time	60 °C	10-100%	252 days
[82]	NMC-LMO	✓	✓	SoC, T, time	30-50 °C	30-90%	290 days
[83]	NMC	✓	✓	SoC, T, time	0-45 °C	25-100%	450 days
[13]	NMC	✓	✓	SoC, T, time	35-50 °C	0-100%	520 days
[84]	NMC	✓	x	SoC, T, time	35-50 °C	0-100%	520 days
[85]	NMC	✓	✓	T, time	10-46 °C	50%	520 days
[86]	NMC-LMO	✓	✓	T, time	30-60 °C	30-100%	1200 days
[87]	NCA	x	✓	SoC, T, time	30-55 °C	90-110%	219 days
[88]	-	✓	x	SoC, T, time	30-60 °C	30-100%	800 days
[89]	-	✓	x	SoC, T, time	0-60 °C	5-100%	9 year

In the following, the impact of these stress factors will be discussed separately. However, it is important to note that their degradation behavior is not entirely independent of one another but is strongly correlated. A summary of all reviewed calendar aging models, including their range of test conditions, is shown in Table II.

1) Time:

a) *Modeling techniques (time):* It is widely reported in the literature that the major degradation effect for graphite anode-based LIBs is the formation and growth of the SEI layer [61], [68], [79], [80], [85], [86]. As mentioned above, SEI layer growth is generally associated with a $\sqrt{\text{time}}$ aging behavior. To this extent, the time dependence of calendar aging is most often modeled using a power-law relationship with z in a range of 0.5–0.8 [68], as shown in the following equation:

$$Q_{\text{loss}} = f(\text{SoC}, T)t^z \quad (1)$$

where

- Q_{loss} lost charge;
- $f(\text{SoC}, T)$ function describing the state of charge and temperature dependence of calendar aging;
- t time;
- z power exponent.

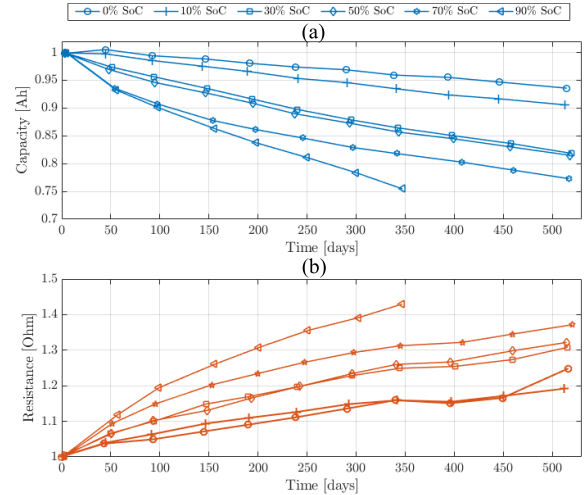


Fig. 7. Normalized (a) capacity and (b) resistance over time for calendar aging test of NMC cells performed at 50 °C and various SoCs [13]. Their results show a clear correlation with SoC, where higher storage level results in higher degradation rate.

An example of a corresponding degradation curve is shown in Fig. 7. The exponential or preexponential components are often functions of SoC and temperature. In general, a higher

TABLE III
OVERVIEW OF STUDIES INVESTIGATING EMPIRICAL AND SEMIEMPIRICAL CYCLE LIFE MODELS

Study	Chemistry	Cap.	Res.	Factors	Conditions				
					Temp.	SoC	DoD	C-rate	Throughput
[94]	LFP	✓	x	SoC, DoD, C, Ah, T	25-40°C	30-70% (avg)	12.5-75%	1-1.82C	900 FEC
[73]	LFP	✓	✓	SoC, DoD, Ah, T	35-50°C	27.5-72.5% (avg)	10-60%	4C	1k-7k FEC
[110]	LFP	✓	x	DoD, C, T	-30-60°C	100% (start)	10-90%	0.5-10C	1k-6.5k FEC
[111]	LFP	✓	✓	DoD, T, C	-18-40°C	100% (start)	20-100%	1-15C	550-2900 FEC
[41]	LFP	✓	x	T, Ah, C	25°C	100% (start)	100%	0.5-5C	550 FEC
[97]	LFP	✓	x	T, Ah, C	25°C	100% (start)	100%	0.5-5C	1.2k-10k
[112]	LFP	✓	x	SoC, T, Ah, C	36-45°C	38.5-60% (avg)	100%	2.82-6C	4k-20k FEC
[113]	LFP	✓	✓	SoC, DoD, T, Ah	30, 45°C	1.25V-2V 3.65V-3.95V	100%	4C	200 FEC
[105]	LFP	✓	✓	DoD, Ah, C	30°C	100% (start)	5-100%	1-3.5C	2k-5.5k FEC
[114]	LFP	✓	x	SoC, Ah, C	55°C	0-30%	10-30%	4-8C	3.9k-12.5k
[115]	LFP	✓	x	C, T	25,45°C	100% (start)	100%	1C	4.5k FEC
[79]	LFP	✓	✓	SoC,DoD, T	35-50°C	10-90% (start)	10-80%	4C	8k
[78]	LFP	✓	✓	C, Ah,	25°C	40-80% (start)	3,6%	0.5-1C	-
[116]	LFP	✓	x	SoC,T, C,Ah	22.8°C - 51.6°C	100% (start)	60,100%	1-4C	654-4286 FEC
[117]	LFP	✓	✓	x	22.8°C - 51.6°C	100% (start)	60,100%	1-4C	654-4286 FEC
[101]	LFP	✓	x	T, C, Ah	40-50°C	60-85% (start)	20-65%	0.4-4C	4k
[42]	LFP	✓	x	SoC,DoD,T, Ah	20°C	75-100% (start)	50-75%	1C	4k-8k FEC
[118]	LFP	✓	✓	SoC, Ah,	5, 44°C	100% (start)	100%	1.5C	990 FEC
[42]	NMC	✓	x	SoC,DoD,T, Ah	20°C	75-100% (start)	50-75%	1C	4k-8k FEC
[118]	NMC	✓	✓	SoC, Ah,	5, 44°C	100% (start)	100%	1.5C	990 FEC
[13]	NMC	✓	✓	SoC, DoD, Ah, T	35°C	10-95% (avg.)	5-100%	1C	1.5-4.5k FEC
[86]	NMC	✓	✓	DoD, Ah, T, C	40,50°C	100% (start)	20-40%	10,20C	-
[84]	NMC	✓	x	SoC, DoD, C, T	-10-50°C	20-80% (avg.)	10-100%	1/3-2C	900-1k FEC
[119]	NMC	✓	x	SoC, T, Ah, C	10-45°C	100% (start)	55-75%	1/3-5C	800-1400 FEC
[93]	NMC	✓	✓	SoC, T, Ah, C	10-45°C	40-70% (avg)	20%	5-20C	-
[120]	NMC	✓	x	SoC, T, Ah, C	10-46°C	100% (start)	50%	0.5-6.5C	1.3k-1.7k FEC
[85]	NMC	✓	x	T, Ah, C	10-46°C	100% (start)	10-90%	0.5-6.5C	900-4.3k FEC
[92]	NMC	✓	✓	SoC, DoD, T, Ah, C	40°C	5-90% (avg)	10,60%	1C	2k FEC
[82]	NMC/LMO	✓	✓	SoC, T	30-50°C	100% (start)	10-70%	4C	-
[101]	NCA	✓	x	T, C, Ah	40-50°C	60-85% (start)	20-65%	18C	4k
[86]	NCA	✓	✓	DoD, Ah, T, C	40,50°C	100% (start)	20-40%	9,16C	-
[121]	NCA	✓	✓	SoC, DoD, Ah, T	20°C	EOCV: 3.9V-4.1V	20-80%	9,16C	-
[122]	NCA	✓	x	SoC, DoD, T	20°C	80,100% (start)	60-80%	-	782 FEC
[123]	NCA	✓	x	DoD, T, Ah, C	0-50°C	EEODV: 2.4-2.5V EOCV: 4.1-4.3V	60-80%	0.2-1C	782 FEC
[42]	LMO	✓	x	SoC,DoD,T, Ah	20°C	75-100% (start)	50-75%	1C	4k-8k FEC
[118]	LMO	✓	✓	SoC, Ah,	5, 44°C	100% (start)	100%	1.5C	990 FEC
[100]	LMO	✓	x	SoC, T,	25°C	35-50% (avg.)	20-95%	1C	900 FEC
[124]	LMO	✓	x	Ah	25°C	100% (start)	100%	1C	700 FEC

TABLE III
(Continued.) OVERVIEW OF STUDIES INVESTIGATING EMPIRICAL AND SEMIEMPIRICAL CYCLE LIFE MODELS

[125]	LMO	✓	x	DoD, T, C	20-50°C	100% (start)	20-100%	1-5C	900 FEC
[126]	LCO	✓	x	SoC, DoD, T, C	25°C	EOCV: 4.1V-4.3V	100%	0.5-1.4C	900 FEC
[127]	LCO	✓	x	DoD, T, Ah, C	25-45°C	100% (start)	20-30%	0.6-1.2C	500-800 FEC
[89]	LCO	✓	x	SoC, DoD, T	0-60°C	0-100% (start)	3-80%	1/5C	10k FEC
[128]	LCO	✓	x	Ah, C	-	100% (start)	100%	0.5-1C	550 FEC
[129]	LCO	✓	x	SoC, C	25°C	EOCV: 4.2-4.35	100%	1C	250-500 FEC

SoC or higher temperature results in an increased calendar degradation rate. At a higher SoC, more lithium is intercalated in the anode resulting in a lower anode potential (V versus Li/Li+)² and higher reaction rate. Similarly, as the particle collision rate increases at higher temperatures, the reaction rate increases. This is confirmed by the results of [13], as shown in Fig. 7. It also shows that, for a lower SoC, the capacity retention follows a more linear curve. Comparable results were observed in [67]–[69], [78], and [87]. A possible explanation for the linear decay is cathode surface film growth, which has a nonpassivation character. Therefore, its reaction rate does not decrease over time³ [88]. Another explanation could be transition metal dissolution as a result of high-temperature storage.

b) *Modeling limitations and challenges (time):* An occasionally observed result is a slight increase in capacity when the cell is still relatively new. This is most commonly observed for lower SoC storage but is also observed under cycling conditions [13], [65], [78], [79], [89]. Again, this is also shown in Fig. 7, for the 0% and 10% SoC lines. After this initial increase in capacity, the capacity fading generally follows a similar trend as for other conditions, and therefore, the found empirical fit is often still valid even though it has been offset by the initial increase. de Hoog *et al.* [79] mention electrochemical milling as a potential cause for the increase in capacity. In [90], the so-called relaxation effect, due to the long resting period after cycling, is mentioned as a possible explanation. This relaxation effect can be caused by a change in local charge equilibrium, a drop in the concentration gradient of active material and electrolyte, and a change in double-layer capacitance structure. Another explanation given in [65] denotes the passive electrode effect as a possible explanation; here, a slow movement of active lithium particles between the passive and active parts of the anode is given as an explanation for the rise in capacity.

c) *Key insights on the effect of time:* The effects of time on the calendar aging of LIBs can be summarized as follows.

- 1) SEI layer growth is reported as the main cause for the degradation rate following a $\sqrt{\text{time}}$ curve. Higher temperature and SoC result in a faster degradation rate.

²Lithium metal composites have a negative potential; therefore, voltages are measured with respect to this potential.

³A material becoming passive means that it is getting less affected or corroded by its environment.

- 2) At lower SoC, the degradation of the cathode might be an explanation for the more linear decay of capacity.
- 3) An initial increase in capacity is occasionally observed. Different explanations for this phenomenon are given in the literature.

2) *Temperature (Calendar):* The most critical stress factor for LIB degradation is temperature; all reaction rates, parasitic and nonparasitic, are related to temperature. It, therefore, affects all other stress factors.

a) *Modeling techniques (temperature (calendar)):* The most common semiempirical technique to model the degradation due to temperature is using the Arrhenius law [69], [78], [87], [91], as given in (2). The Arrhenius law models the effect of temperature on chemical reaction rate

$$k = A \exp \frac{-E_a}{RT} \quad (2)$$

where

- k reaction rate constant;
- T absolute temperature;
- A preexponential factor;
- E_a activation energy;
- R universal gas constant.

The activation energy here refers to the additional energy required for a reaction to take place. The Arrhenius equation is often related to the rate of all parasitic side reactions, leading to SEI growth [21] in LIB aging research. Other models based on exponential or power-law relationships are also often utilized [34], [81].

b) *Modeling limitations and challenges (temperature (calendar)):* Based on the summary of the testing conditions presented in Table II, it is clear that the majority of the papers have investigated accelerated calendar aging at elevated temperatures, ranging from 30 °C to 60 °C. This is probably done to reduce the calendar life to a better manageable period. However, this raises the question of whether the aging rate at 50 °C–60 °C is translatable to the aging rate at 15 °C–25 °C. A rule of thumb is that the aging rate doubles for every 10 °C increase in temperature [13], [68], [81], [87], [91]. For studies using the Arrhenius law, this would result in activation energy close to 50 kJ/mol. In some cases, this assumption is even used to derive the aging model [92]. To test this hypothesis, the aging data of the reviewed studies are sampled and analyzed according to

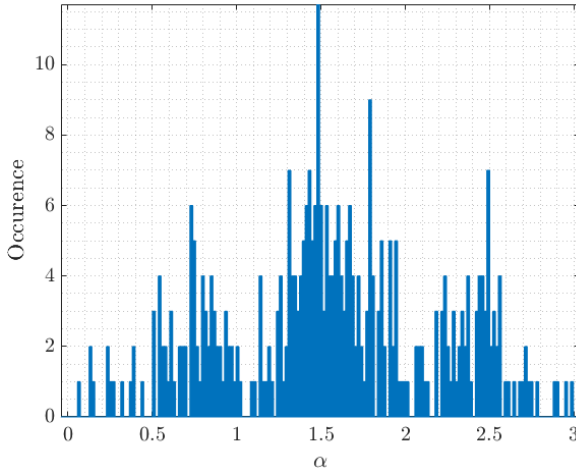


Fig. 8. Found results for α of (3). In the tested studies, 60% of calculated values of α were below 2, and a peak around alpha = 1.5 was observed, which means that most tested cells have an increased aging rate of 50% for every 10° increase. The spread of values confirms the interdependence with other stress factors, such as age and SoC; however, no clear correlation was found.

the following equation:

$$\alpha = \frac{C(T_2)}{C(T_1)} \frac{10}{T_2 - T_1} \quad (3)$$

where

- $(C(T_2)/C(T_1))$ ratio of percentage capacity loss between temperatures;
 $T_{1,2}$ temperatures of samples 1 and 2;
 α factor to test the hypothesis.

An α equal to 2 would indicate twice as much capacity degradation for every 10 °C. Using (3), the data of each study are compared, only to cells from the same study, tested at the same SoC, and measured around the same time, such that only the temperature is variable. Fig. 8 concludes that the given hypothesis often overestimates the calendar aging, as the peak occurs at approximately $\alpha = 1.5$, which means that most tested cells increase aging by 50% every 10 °C. Further investigation did not show any other correlation between age and SoC.

Due to the complex nature of LIB degradation, it is challenging to give a rule of thumb figure as the aging rate will always depend on multiple correlated factors. For this reason, the testing conditions, especially temperature, should be as close as possible to the operating conditions of the application, as extremely high temperatures result in different aging mechanisms and, therefore, different aging behaviors. An example of this is shown in [81]. Here, the authors show that, for an NMC cell stored at a temperature of 60 °C, the aging rate increases tenfold when the cells are stored at 100% SoC compared to 20% SoC. In comparison, this difference at 30 °C is negligible. A possible explanation could be the restructuring of the SEI layer as it starts to break down at higher temperatures, dissolves, and reprecipitates. Furthermore, in [21], it is also reported that organic SEI products are changed into more stable inorganic products, thereby reducing the reaction rate but also reducing the ionic conductivity of the SEI and thus increasing the resistance.

c) *Key insights on the effect of temperature (Calendar Aging):* The effects of temperature on the calendar aging of LIBs can be summarized as follows.

- 1) The Arrhenius law (or similar exponential forms) is the most common form of modeling the temperature dependence of calendar aging.
- 2) The temperature has a strong influence on all other stress factors and aging mechanisms. To this extend, test conditions should be as close as possible to operating conditions in order to avoid modeling errors.
- 3) *State of Charge (Calendar):* The last stress factor related to calendar aging is the SoC (or analogously terminal voltage). Table II shows strong similarities between studies regarding testing conditions since most studies have modeled the effect of SoC based on three to four conditions.

a) Modeling techniques [SoC (calendar)]:

Eddahach *et al.* [75] have modeled the SoC dependence as a polynomial function, where the interdependence of temperature and SoC is included by multiplication, as shown in the following equations:

$$G(t) = A(T, \text{SoC})e^{B(T, \text{SoC})t} + Ce^{Dt} \quad (4)$$

with

$$A(T, \text{SoC}) = a_1 \cdot \text{SoC} + a_2 \cdot T + a_3 \cdot \text{SoC} \cdot T \quad (5)$$

$$B(T, \text{SoC}) = b_1 \cdot \text{SoC} + b_2 \cdot T + b_3 \cdot \text{SoC} \cdot T \quad (6)$$

where

- $G(t)$ calendar aging over time;
 SoC state of charge;
 T temperature;
 $A(T, \text{SoC})$ and $B(T, \text{SoC})$ functions to model temperature and SoC interdependence;
 a_{1-3}, b_{1-3}, C , and D curve fit parameters.

In [34] and [93], calendar aging is modeled as exponentially dependent on SoC, as follows:

$$A_{\text{cal}} = A_0 e^{\frac{\text{SoC}-\text{SoC}_0}{b}} \cdot A_0 e^{\frac{T-T_0}{c}} \sqrt{t} \quad (7)$$

where

- A_{cal} calendar lifetime;
 A_0 specified calendar lifetime under conditions SOC_0 and T_0 ;
 b and c curve fit parameters.

Equation (8) shows how Redondo-Iglesias *et al.* [67], Wright *et al.* [94], Rechkemmer *et al.* [95], and Petit *et al.* [96] modeled the preexponential factor in the Arrhenius law to be SOC-dependent. Redondo-Iglesias *et al.* [67] and Wright *et al.* [94] also model the activation energy to be dependent on SoC, as follows:

$$Q_{\text{loss}}(t, T, \text{SoC}) = Ae^{B \cdot \text{SoC}} \cdot e^{\frac{-E_a + C \cdot \text{SOC}}{kT}} t^z \quad (8)$$

where

- Q_{loss} lost charge;
 A, B , and C curve fit parameters;
 k gas constant;
 T temperature.

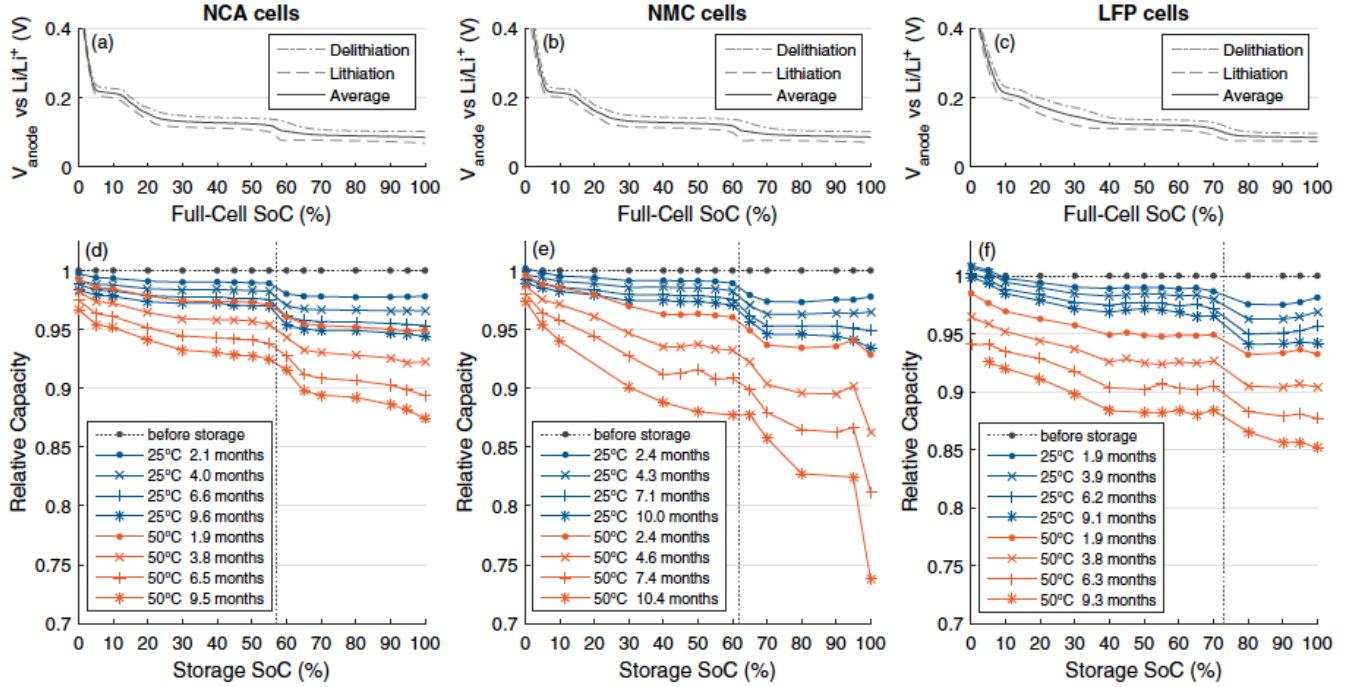


Fig. 9. (a)–(c): Graphite anode potential versus SoC for an NCA, NMC and LFP cell respectively. (d)–(f): Rate of degradation of the corresponding cells for various temperatures.⁴ A strong correlation between anode potential and degradation rate is observed for all cells, especially, the phase transformation around 60%–70% marks a significant change in degradation rate. The figure is obtained from the publicly available material of Keil *et al.* [36], under the Creative Commons Attribution 4.0 License CC-BY.

Grolleau *et al.* [69] observed a linear increase for the SoC-dependent degradation. Therefore, the kinetic dependence of (T, SoC) is modeled using an Arrhenius equation multiplied by SoC. The SoC dependence of calendar age-induced capacity degradation is modeled as a power-law relationship in [68], [74], [84], and [91]. In contrast, the decrease in power capability is modeled in a linear relationship in [74].

Although diverse modeling methodologies are documented in the literature, the general trend suggests an increase in degradation with increasing SoC, especially at higher temperatures [13], [81].

b) Modeling limitations and challenges [SoC (calendar): Most reviewed studies only perform tests with three to four different SoC conditions due to practical constraints on testing capacity. This incorrectly leads to the belief that the rate of capacity and resistance deterioration for higher SoC's increases continuously. However, in [36] and [91], calendar aging was investigated with a higher resolution in SoC. Both these studies found a direct correlation between the graphite anode potential and capacity aging.

In Fig. 9, the results of [36] are shown for three different chemistries. As expected, an increase in storage temperature increases the capacity fading. However, more importantly, the results also show different plateaus with respect to storage SoC. There seems to be a direct correlation between the rate of capacity fading and the graphite anode stages for all three chemistries. These stages occur due to the different compositions of the lithium and carbon molecules, resulting in a different volume and potential. A schematic representation

of the different stages, along with the anode potential during charge and discharge, is shown in Fig. 10 [97].

The results of [36] and [88] confirm that SEI growth results from electrochemical instability of the electrolyte-electrode interface. In both studies, these plateaus were not observed in the resistance increase. For the LFP cell, this increased independently of SoC, whereas the rate of resistance increase for the NMC and NCA cells was found to be substantially larger at higher SoC, especially around 90%–100%. The cathode surface film layer could be a possible explanation, which, for LFP cells, is much less SoC-dependent due to the more stable crystal lattice and two-phase regime. Based on the results of [36] and [91], it can be concluded that the curve fitting the SoC dependence with only three test conditions is insufficient to accurately capture capacity fade as a function of SoC, as it will lead to significant underestimation and overestimation in certain SOC regions. The advantage, however, is that the anode potential can be determined prior to performing the aging test. For example, the anode potential or differential voltage analysis (DVA) can be used. Once the anode potential is known, the choice of SoC testing conditions can be made strategically. Furthermore, knowing where the phase transition occurs during the operation of an LIB can help reduce calendar aging.

Another observation on the results shown in Fig. 9 is the drastically increased aging at 100% SoC for the NMC chemistry. This was not observed in the other chemistries, and similar results have been found in other aging studies of NMC cells [79], [81], [87], [91]. The increased aging appears to be independent of anode potential. A possible explanation could be other degradation mechanisms driven by

⁴Half-cells are separated cells with only an anode or cathode.

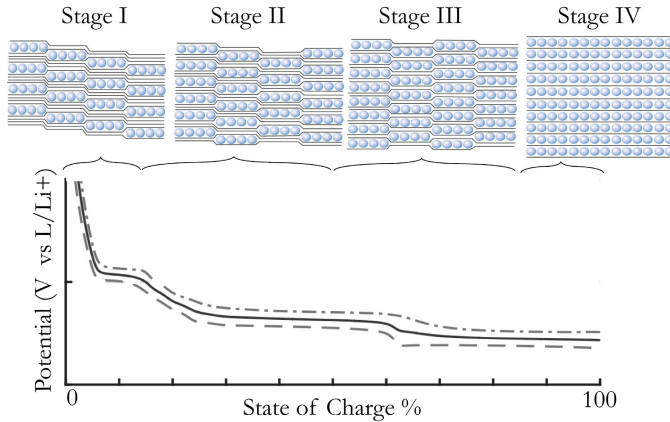


Fig. 10. Schematic representation of the staging phenomena observed at the anode [97]. Because the arrangement of carbon and lithium molecules differs in each phase, each stage has a different potential and volume and, therefore, a different degradation rate.

a high cell voltage, such as electrolyte oxidation, transition metal dissolution, or structural damage to the cathode due to a high degree of lithiation [98], [99]. Due to the disproportionate increase in aging at high temperature and very high SoC ($\geq 95\%$), it is not recommended to test NMC cells at 100% SoC if the amount of testing conditions is limited as it will result in large overestimations for conditions below 95% SoC.

c) Key insights on the effect of SoC (calendar aging): The effects of SoC on the calendar aging of LIBs can be summarized as follows.

- 1) The anode potential appears to be the main factor determining the rate of degradation in graphite-anode-based cells. This demonstrates that SEI layer growth is the dominant aging mechanism for these cells.
- 2) Modelers should be cautious when developing models based on a limited number of testing conditions because the degradation rate is determined by the anode potential, which is not a continuously changing potential but instead follows the stages determined by the anodes' phase transitions.
- 3) A significant amount of studies testing NMC cells at 100% SoC observed a disproportionate increase in aging, for a slightly lower SoC. To this extent, higher accuracy over the entire SoC range can be achieved when the maximum SoC tested is 90%–95%.

B. Cyclic Aging

Table III summarizes the cycling aging studies and their testing conditions. The relevant part is discussed in the accompanying section for studies that discuss both calendar aging and cyclic aging.

1) Combining Cyclic Aging and Calendar Aging: Based on the reviewed studies, no single idea about the correlation between calendar aging and cyclic aging can be derived. In [81], aging is modeled using Dakin's approach. Here, cyclic aging and calendar aging are modeled to be multiplicative. Schmalstieg *et al.* [13], Vetter *et al.* [21], Bloom *et al.* [21], and Guenther *et al.* [93] have mentioned that cycling results in additional (cyclic) degradation due to added mechanical stress

and lithium plating. Furthermore, various studies show that the SEI layer's growth and morphology alter according to the operating conditions. During cycling conditions, the SEI layer stays more porous, whereas a much denser layer is formed under storage conditions [42], [43], [91], while cyclic aging and calendar aging are mentioned to have a strong superposition for high temperatures or high SoC in [91] and [100]. For milder conditions, especially at lower temperatures and increased C-rate, cycling aging is probably dominant.

Note that studies that only discuss cyclic aging have inherently incorporated calendar aging as well. In this case, the superposition of calendar aging is assumed to be nonexistent [93], [101] or negligible compared to the cycling-induced aging. However, in these cases, the fast sequential cycling tests mask the effect of calendar aging and, therefore, lead to estimation errors in applications with significantly more time between cycles. In practice, every modeler should determine the best practice for themselves, depending on their application and operating conditions.

2) Addressing Irregular Cycles (Rainflow Counting Method): Often, cyclic aging studies are performed under fixed conditions. However, in reality, aging is not as static as these test conditions. One way of dealing with highly irregular power profiles is using the rain flow counting method. Rainflow counting is a common fatigue analysis technique used to calculate the combined fatigue of a summation of different stress cycles. Several studies have used the rain flow counting method to calculate the combined degradation of an irregular power profile [39], [68], [89], [102], [103]. An example of this is shown in Fig. 11. Here, the rainflow matrix is shown for a randomly generated load profile, which shows the number of cycles of a particular current rate [A] and throughput [$A*s$]. Other output quantities could be the depth of discharge (DoD), average SoC, or idle time. Next, the degradation can be determined based on the number of cycles with a specific amount of stress. The advantage of this technique is that it allows assessing the degradation of irregular profiles more accurately. However, it assumes that the sequence of cycles does not influence the outcome, e.g., the degradation due to a high DoD cycle followed by a low DoD cycle is similar to a low DoD cycle followed by a high DoD cycle. Furthermore, it assumes that the effect of a particular cycle (or sum of cycles) is independent of the current age of the battery. Interested readers are directed to [104] for more information on the rain flow counting technique.

3) Throughput: The throughput describes the net Ah delivered by the battery over multiple cycles. As a result, it is one of the critical stress factors for cycling aging.

a) Modeling techniques (throughput): Similar to time for calendar aging, the relationship for throughput is often modeled using a power-law relationship [13], [38], [96], [105], [107], as described in (9) or (10). Furthermore, throughput is also modeled in terms of number of cycles combined with depth of discharge. Often, with similar power-law equations [68], [79]

$$Q_{\text{cycl}} = f(\text{SoC}, T, \text{DoD}, I) A h^z \quad (9)$$

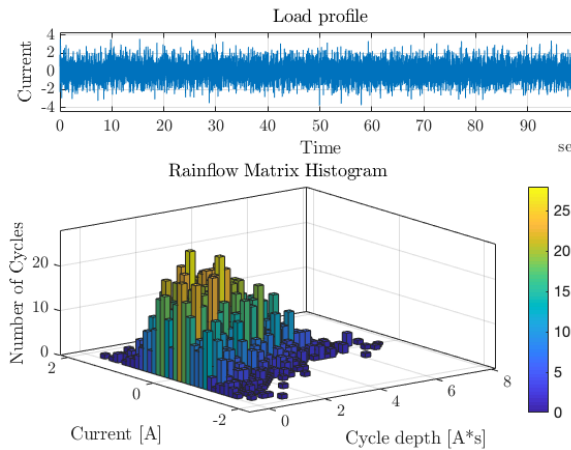


Fig. 11. Example of a rainflow matrix histogram based on a randomly generated load profile. In this case, the rainflow matrix counts the number of cycles of a specific cycle-depth with a specific current load.

$$Q_{\text{cycl}} = f(\text{SoC}, T, \text{DoD}, I) N_{\text{cycle}}^z \quad (10)$$

where

- $f(\text{SoC}, T, \text{DoD}, I)$ degradation due other stress factors;
- Ah total cumulative throughput of the cell;
- N_{cycle} amount of performed cycles, sometimes expressed in terms of depth of discharge;
- z power-law exponent.

The typical values of z are in the range of 0.5–0.8, which is generally associated with SEI layer growth. Schmalstieg *et al.* [13] found the best fit for z around 0.5, after subtracting calendar aging. Meaning that as the battery ages, the SEI thickens, and the capacity fades due to cycling-induced stress on the SEI decreases. In [122], values of z in the range of 0.8 have been reported, following a less logarithmic and more linear degradation rate. A possible explanation could be an increased share of cathode surface layer film growth [88]. Todeschini *et al.* [109] found the best curve fit using $z = 1.23$. Here, the degradation due to the charge-sustaining (CS) mode of plug-in hybrid EVs (PHEVs) has been investigated. Here, the CS mode of a PHEV was characterized by low SoC and very high C-rates. The resulting degradation showed an increasing degradation rate, resulting in an exponential factor $z > 1$. Because of the low SoC, combined with the high C-rate, this increasing degradation rate is potentially dominated by metallic lithium plating, which, in contrast to SEI growth, is a self-reinforcing process.

However, not all studies have reported nonlinear cyclic aging characteristics. In [89] and [92], the cyclic degradation is modeled as linearly increasing with throughput even though the results show a very slight saturation. Furthermore, in [117], cycling aging is assumed to be linearly dependent on the number of cycles. This is, however, not confirmed by the experimental data shown in this article. Finally, Hall *et al.* [42] have found a linear correlation between cycling-induced

capacity fade and the number of cycles (on top of a $t^{0.5}$ time dependence). A destructive physical analysis showed that damage to the cathodes' active material was the leading cause for the cycle-induced aging. In addition, Hall *et al.* [42] observed a linear increase in resistance, whereas the capacity fading showed a $t^{0.5}$ correlation. This indicates that the degradation mechanisms between capacity fade and resistance increase are different [13]. This difference between capacity and resistance deterioration was found in several studies [68], [91], [106], [114]. Unfortunately, no explicit explanation for this observation was given.

b) Modeling limitations and challenges (throughput):

For studies investigating only cyclic aging [68], [95], [105], [107], [114], it could be argued that the superposition of calendar aging has a strong effect on their results, especially at higher temperatures and SoC. According to [105] and [122], time is inherently incorporated in throughput, as every charging instance with a particular C-rate is also a function of time. However, this is only valid if the cell is cycled continuously, which is rarely the case in practical applications.

Most of the above-described studies use some form of the Arrhenius equation, combined with a power-law relationship on throughput or number of cycles. This form of modeling is generally well suited to predict aging due to long term storage or cycling during a postprocess calculation. However, for online calculations over a shorter period or fast-changing operating conditions, it is less suited as the current age of the battery is not taken into account at every new iteration/calculation. This has been resolved by Petit *et al.* [96] by differentiating the Arrhenius/power-law over time. Starting with (11), this results in the linearized form, as shown in (12) [96]

$$Q_{\text{loss}} = B(I) \exp \frac{-E_a + \alpha|I|}{RT} Ah^z \quad (11)$$

$$\frac{dQ_{\text{loss}}}{dt} = f(I, T) \left(\frac{Q_{\text{loss}}}{B(I) \exp \frac{-E_a + \alpha|I|}{RT}} \right)^{1-\frac{1}{z}} \quad (12)$$

with

$$f(I, T) = \frac{|I|}{3600} z B(I) \exp \frac{-E_a + \alpha|I|}{RT} \quad (13)$$

Another limitation of the Arrhenius/power law is that it only captures the degradation in the first stages of battery life, during which the degradation rate decreases as the battery ages. However, at a certain age, all LIBs experience an increase in degradation rate due to lithium plating, as shown in Fig. 5. de Hoog *et al.* [79] model this inflection point as a polynomial equation based on the number of cycles and DoD according to (14). Fig. 12 shows that this results in a good fit on their aging data and shows the inflection points that start to occur around 3000 cycles. However, note that this is not observed in the data, and therefore, the age at which plating starts to occur remains unknown

$$\text{RCD}(x, y) = \sum_{i=0, j=0}^{n, m} a_i x^i + b_j y^j \quad (14)$$

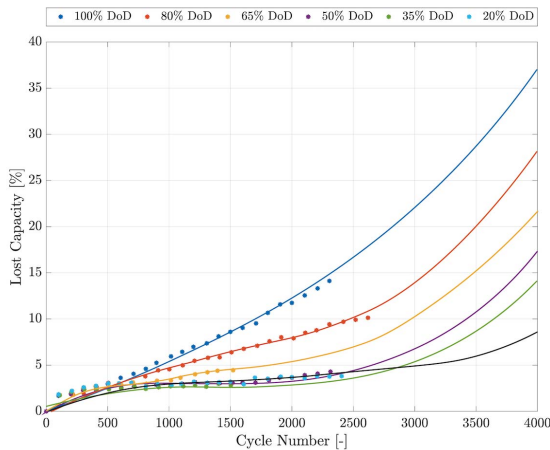


Fig. 12. Aging and fitting result from [79]. In contrast to many exponential models, this polynomial model takes into account the increasing degradation rate at later point in battery life due to lithium plating.

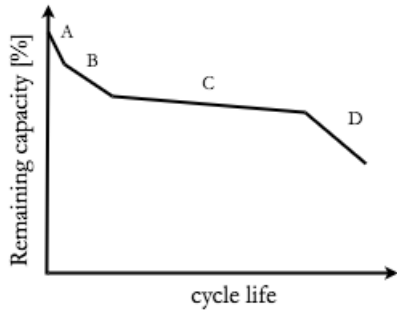


Fig. 13. Modeling battery degradation based on four different linear stages [stages (A)–(D)], this allows to linearize the degradation model over the entire lifetime of the battery [39].

where

- RCD relative capacity degradation (%);
- x full equivalent cycle number;
- y DoD (%);
- a_i constants for x ;
- b_j constants for y ;
- n order of x ;
- m order of y .

Another option is to linearize the various stages seen in LIB life, such as done in [39]. Here, the authors distinguish between four different stages, each modeled as linear functions dependent on various stress factors (see Fig. 13).

c) *Key insights on the effect of throughput:* The most important insights on the effect of throughput can be summarized as follows.

- 1) Often, an Ah^z relationship, with $0.5 \leq z \leq 1$, is found for studies modeling the effect of throughput on cyclic aging. Even though this may result in good accuracy in the first stages of battery life, it fails to capture the degradation in later stages, where an increased degradation rate is generally observed after an inflection point.

2) Studies investigating only cyclic aging inherently include the effects of calendar aging in their models. Depending on the application of the model, this can potentially lead to inaccurate results. Other studies have subtracted the expected amount of calendar aging from their cyclic aging test results to more accurately curve the aging due to cycling.

4) Temperature:

a) Modeling techniques [temperature (cyclic)]:

Also, for cycling aging, the Arrhenius law [13], [38], [39], [79], [87], [105] or similar exponential relationships [68], [81], [92] are most often used to model the temperature dependent reaction rate. An example of an Arrhenius law model is given in (11). Also, polynomial relationships, such as the example given in (15) and (16), are occasionally used [80]

$$Q_{\text{loss}} = B_1(T)e^{B_2(T)I_{\text{rate}}} Ah \quad (15)$$

with

$$B_1(T) = aT^2 + bT + c, \quad \& \quad B_2(T) = dT + e \quad (16)$$

where

- | | |
|-----------------------|-----------------------|
| Q_{loss} | lost capacity; |
| T | temperature; |
| I_{rate} | C-rate; |
| Ah | throughput; |
| $a, b, c, d,$ and e | curve fit parameters. |

b) *Modeling limitations and challenges [temperature (cyclic)]:* In the studies mentioned above, good accuracies are achieved when using the Arrhenius law to model the temperature dependence at temperatures above room temperature. However, different from calendar aging, the Arrhenius law is not a good indicator for the temperature-dependent degradation rate at temperatures below room temperature [39], [81], [89] (and occasionally also at higher temperature rates [122]). For calendar aging, lower temperatures reduce the reaction rate of parasitic side reactions; under cycling conditions, the lower temperatures also reduce the battery's ionic conductivity, leading to an increased impedance and reduced performance [125]–[127].

In [122] and [128], a temperature around a 20°C – 25°C was found to be the dividing limit at which the impedance starts increasing for lower temperatures, and above which the impedance decreases for lower temperatures. As a result, the least (cyclic) aging is generally observed at around 20°C – 25°C [79], [81], [89], [105], [106]. An example of this is shown in Fig. 14, where the preexponential and exponential factors $B_1(T)$ and $B_2(T)$ from (15) and (16) are shown [80]. Therefore, cycling aging models utilizing exponential relationships, fit on test results above room temperature, can often not be used for conditions below a 20°C as this would result in severe underestimations. Nevertheless, the Arrhenius law can also be used at lower temperatures if combined with positive activation energy. An example obtained from [118] and [129] is shown as follows:

$$Q_{\text{loss}} = A_L e^{\frac{E_L}{RT}} + A_H e^{-\frac{E_H}{RT}} \quad (17)$$

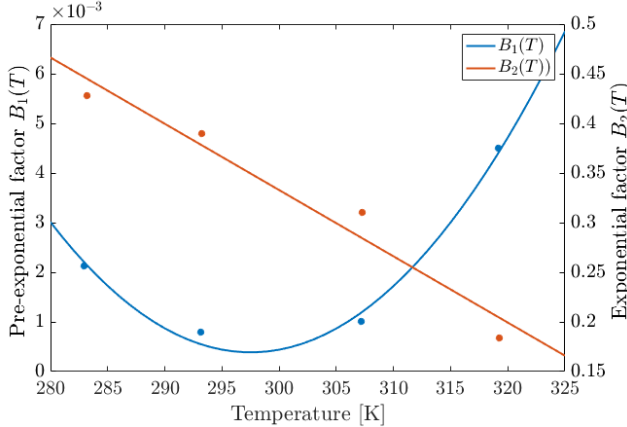


Fig. 14. Preexponential and exponential factors $B_1(T)$ and $B_2(T)$ from (15) show that the lowest degradation rate is observed for temperatures around room temperature. In addition, a decreasing $B_2(T)$ shows that the effect of current rate decreases at higher temperatures. The shown results are obtained for NMC-LMO cells cycled at 50% DoD and 1 C.

where the letters H and L denote the found parameters for high and low temperatures.

Waldmann *et al.* [128] showed, using postmortem analysis, that different aging mechanisms are dominant above and below 20 °C for an NMC-LMO blended cathode cell. Their results show that lithium plating is the dominant aging mechanism at low temperatures, caused by an increasing polarization near the electrode due to the slow diffusion and low ionic conductivity [43], whereas, at higher temperatures, transition metal dissolution and SEI growth are the dominant aging mechanisms. Similar results have been found in [130] for LCO cells.

A couple of studies have even performed aging tests at subzero temperatures. However, most of them have not included these results in their models due to the extremely short cycle life (below 100 equivalent full cycles) [43], [79], [89], [105]. Huang *et al.* [126] showed that the anode's diffusion rate is the main limiting factor at temperatures below zero. At temperatures above 20 °C, the intercalation potential of graphite anodes often prevents lithium plating [130], until a certain age. At higher temperatures, active material loss and SEI growth are dominant [58], [75]. Especially, cathode chemistries containing manganese are sensitive to higher temperatures (and higher SoC) due to Mn-dissolution.

Not only the effect of temperature changes around 20 °C–25 °C but also the interdependence of temperature with other stress factors, such as C-rate. At higher temperatures, the impact of C-rates becomes less significant, as shown in Fig. 14, and the effect of calendar aging becomes more pronounced [81], whereas, for lower temperatures, the detrimental effect of C-rate increases [80], [81]. More on this is discussed in Section III-B5.

c) *Key insights on the effect of temperature (cyclic):* The most important insights on the effect of temperature can be summarized as follows.

- 1) The majority of papers model the degradation rate to be exponentially dependent on temperature.

- 2) Temperatures around 20 °C–25 °C are a tipping point below which a lower temperature increases the impedance and above which a higher temperature increases the battery's impedance.
- 3) As a result, models utilizing an exponential relationship to model the temperature dependence for cells cycled above room temperature might lead to significant underestimations when used for temperatures below room temperature. A possible solution could be to use both positive and negative activation energies (or exponential factors).

5) *C-Rate:* The C-rate or the rate of (dis)charge is defined as the ratio of power (W) to energy capacity (Wh). Generally, higher C-rates are believed to be more detrimental to battery degradation. This has been confirmed in the majority of the reviewed studies, for C-rates above 2–3 C. Ning *et al.* [131] cycled LCO cells with 1, 2, and 3 C at room temperature. Using an electron microscope and impedance analysis, they showed that the increasing C-rates caused structural damage on the graphite anode of an LCO cell, resulting in the crack and repair of the SEI layer. The rate of capacity and resistance degradation was proportional to the C-rate. Similar results were found in [121] and [122].

a) *Modeling techniques (C-rate):* In [80], [81], [106], [107], and [115], among other studies, the authors modeled an exponential increase in degradation with respect to C-rate, often combined with an Arrhenius like equation, where the activation energy (or, in general, the exponential component) is modeled as a linear function of C-rate, as shown in (11) [96]. Others also included a linear dependence on the C-rate in the preexponential factor [115], [122], as shown in the following equation:

$$Q_{\text{loss}} = A(C)e^{\frac{-E_a(C)}{RT}}n^{0.74} \quad (18)$$

with

$$A(C) = e^{ac^2+bc+c} \quad (19)$$

$$E_a(C) = xe^{yC} + z \quad (20)$$

where

Q_{loss}	lost capacity;
T	temperature;
C	C-rate;
Ah	number of cycles;
a, b, c, x, y , and z	curve fit parameters.

Lam and Bauer [89] and Millner [92] inherently incorporated C-rate by using the normalized standard deviation in SoC ($\text{SoC}_{\text{dev}}(t)$) per time unit, as shown in (21) and (22)

$$Q_{\text{loss}} = k_1 \text{SoC}_{\text{dev}} \exp k_2 \text{SoC}_{\text{avg}} + k_3 \exp k_4 \text{SoC}_{\text{dev}} \quad (21)$$

where

$$\text{SoC}_{\text{dev}} = \sqrt{\frac{3}{\Delta Ah_m} \int_A h_{m-1}^{Ah_m} (\text{SoC}(Ah) - \text{SoC}_{\text{avg}})^2 dAh} \quad (22)$$

where

- SoC_{dev} normalized deviation in SoC;
- SoC_{avg} average SoC of a cycle;
- ΔAh_m amount of charge processed in cycle m ;
- k_{1-4} curve fit constants.

A different approach was taken in [107] (LFP), for C-rates of 2, 20, and 28 C at temperatures above 36 °C. The authors model the effect of C-rate to be more detrimental than temperature and SOC. Furthermore, according to their model, the impact of the C-rate increases at higher temperatures. However, no accompanying data are shown to verify this. Note that the effect of cell self-heating becomes very significant at these C-rates, leading to increased calendar aging due to significantly elevated cell temperature. Some authors even neglect the effect of C-rate, as it is incorporated in the temperature dependence [39]. This might be a valid assumption for lower C-rates, but, for very high C-rates, the effect of mechanical and kinetic stress might be nonnegligible.

b) *Modeling limitations and challenges (C-rate)*: Before discussing any limitations and challenges regarding C-rate-dependent degradation, the authors would like to point out the differences between chemistries. LFP cells, for example, are well-known for their ability to handle large amounts of power. Furthermore, LIBs using LTO anodes can sustain extremely high C-rates with negligible degradation. However, when conducting cyclic aging tests, readers and modelers should be aware of the effect of energy density on the C-rate. As for the same cell size, with each equal electrode surface area, higher current densities are experienced for cells with a higher energy density for the same C-rate, potentially leading to an unfair comparison between cell chemistries [36].

Although most of the reviewed studies found an exponentially increasing degradation rate at C-rates above 2 C, a significant part found a negligible increase in degradation for C-rates below 2 C and temperatures between 30 °C and 45 °C, for both LFP and NMC chemistries [43], [79], [89], [100], [105], [114], [115], [120]. In [43], the increase in C-rate from 1 to 2 C was found negligible at 45° but nonnegligible at 20 °C, showing the temperature dependence on C-rate. The authors report that the increased reaction rate and ion diffusion kinetics at these temperatures might reduce the stress caused by an increasing C-rate.

To this extend, to adequately explain the effect of C-rate, a distinction between above and below room temperature should be made. At lower temperatures, the ionic conductivity and intercalation rate decrease [105], whereas the higher current density as a result of higher C-rate requires faster diffusion kinetics [43]. As a result, lower temperatures accelerate the detrimental effects of increasing C-rate, resulting in increased mechanical and kinetic stress on the electrodes and an increasing polarization gradient, potentially leading to lithium plating [132]. Similarly, the effect of C-rate often decreases for increasing temperatures, as was found by Wang *et al.* [80]. Their results are shown in Fig. 15. At 10 °C, it shows a clear dependence on C-rate, whereas, for an ambient temperature of 34 °C and 43 °C, the difference between

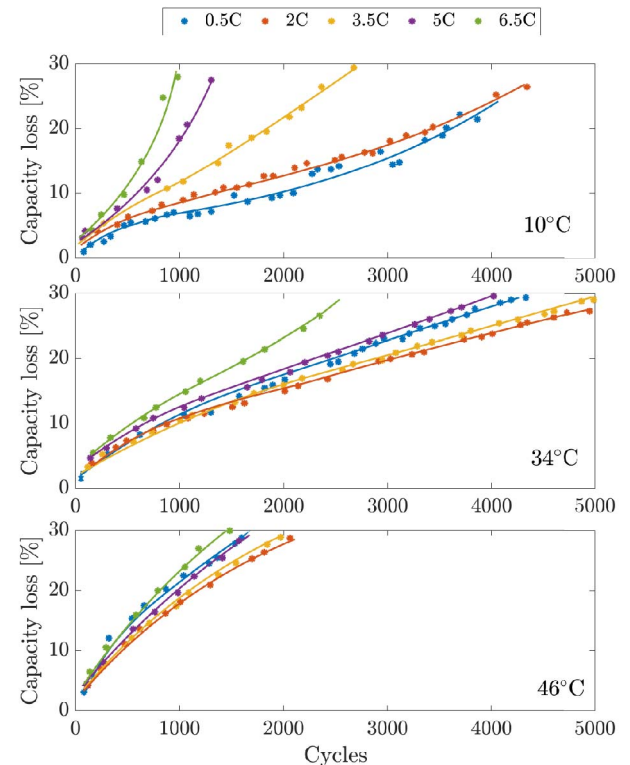


Fig. 15. Cycling aging results of the NMC studies in [80]. The results show the interdependence of C-rate and temperature. At temperatures of 34 °C and 46 °C, the effect of C-rate decreases, and the least aging is observed for 2 and 3.5 C.

C-rates decreased. Also, the capacity retention trajectory is distinctly different at 10 °C and higher C-rates, pointing to an increasing rate of lithium plating. Finally, it is also noteworthy that the least aging is not necessarily observed at the lowest C-rates.⁵ Nevertheless, also at higher temperatures, the effect of C-rate can cause detrimental effects, such as crack propagation of the SEI layer, cathode overcharge (as a result of an increasing polarization gradient), or structural damage to the anode and the cathode, such as graphite exfoliation [31], [133]–[135].

Some authors have accounted for the interdependence between C-rate and temperature. In [81], NMC and NCA cells were cycled at temperatures of 40 °C–50 °C and C-rates of 10 and 20 C. The authors found an exponentially increasing degradation rate for higher C-rates. However, decreasing at higher temperatures, the temperature-dependent C-rate effect was modeled as a linear function of temperature, as shown in (23). Similar methods have been used in [80]

$$k_C = \exp(a(T)I) \quad (23)$$

⁵More studies report less degradation at higher C-rates. In [100] (NMC), at 60% DoD, the least degradation was observed for 3.5 C, followed by 1 C than 2 C, whereas, at 100% DoD, no difference was observed between 1 and 2 C, and only a small difference was observed for cells tested with 10% DoD. All cycling tests were performed at 30 °C. A complex correlation between C-rate and DoD was found; the authors mention that further investigation is required to determine this correlation.

where

- k_C C-rate-induced cyclic aging;
- $a(T)$ linear expression to describe temperature dependence of C-rate;
- I C-rate.

c) *Key insights on C-rate:* From the above-described results, several conclusions can be drawn:

- 1) The effect of C-rate is often modeled to be exponentially dependent.
- 2) A strong interdependence with temperature is observed. Therefore, models obtained using temperatures above 20° are likely not to be valid at temperatures below this threshold due to an increasing impedance.
- 3) For temperatures above 20°, the effect of C-rate decreases. Some studies even report that less aging is observed at higher temperatures or higher C-rates. Modeling C-rate as a temperature-dependent function can, therefore, increase accuracy.
- 4) When performing cycling tests at very high C-rates, cell self-heating should be taken into account.
- 5) Readers and modelers should be cautious when using exponential relationships with respect to C-rate, at C-rates below 2. Several studies have shown that this relationship is not valid for C-rates below the 2-C threshold.
- 6) *State of Charge (Cyclic):* Table III demonstrates that a considerable amount of studies did not investigate the effect of SoC on cyclic aging but, instead, always start their cycle at 100%. These studies are likely to have a larger calendar aging superposition. In addition, users should check whether this is suitable for their application, as battery management systems do not always charge the cells up to this point. The reviewed studies are divided into two categories: 1) studies investigating the influence on end-of-charge voltage (EOCV) and 2) studies investigating the influence of average SoC.

a) *Modeling techniques (end-of-charge voltage):* The final voltage at which the battery is maintained during the constant voltage (CV) charging region is the EOCV. In [131], it was found that 90% of cycling losses resulted from the CV charging region. In [108], [116], [118], [121], and [124], the effect of EOCV was investigated for LFP, LCO, and NCA chemistries. In these studies, the EOCV ranged from 4.1 to 4.3 V, and all studies concluded that a higher EOCV leads to increased aging. According to Su *et al.* [118], a high cell voltage causes a higher potential in the cathode and a lower potential in the anode, which increases the electrolyte oxidation and reduction rates at the cathode and the anode, respectively, resulting in surface film layer formation. Furthermore, in [121], a significant increase in degradation was found with an EOCV of 4.3 V compared to 4.1 and 4.2 V, respectively. The results of [121] are shown in Fig. 16. Based on a DVA, the authors conclude that lithium plating is the cause of the increased degradation rate. At this very end of the charging process, the reduced diffusion capability of lithium into the graphite anode is said to cause lithium plating.

All of the above mentioned studies use different methods to model the degradation due the EOCV or EODV. Li *et al.* [108]

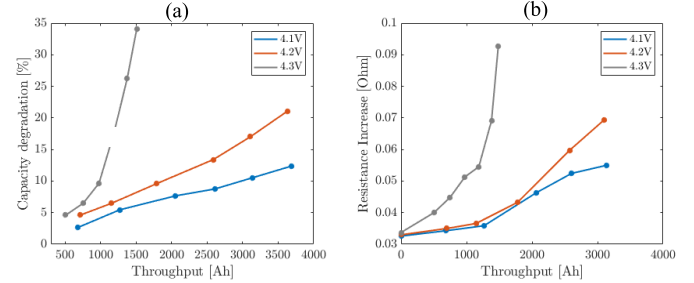


Fig. 16. Comparison of (a) capacity degradation and (b) resistance increase of LCO cells tested at 1 C, 25 °C, and various EOCVs. Significant increase in degradation is observed for the cells cycled up to 4.3 V, and therefore, too high EOCV should be avoided. Based on data obtained from [121].

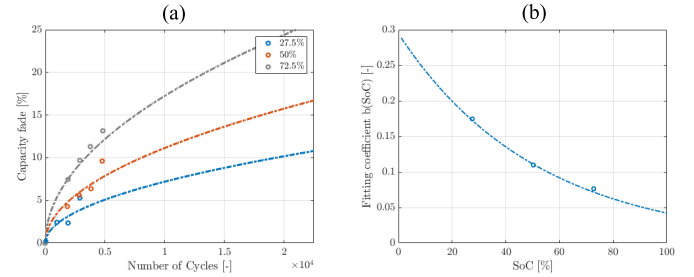


Fig. 17. (a) Aging results for three different cells cycled with 35% DoD and 4 C at 42.5 °C around an average SoC of 27.5%, 50%, and 72.5%. (b) Curve fitting coefficient $b(\text{SoC})$ in (24) for the three different aging tests. Based on data obtained from [68].

develop an aging model based on the addition of multiple single factor stress models. The total cycle life CL is calculated according to the following equation:

$$\text{CL} = \frac{1}{\text{SSF}_0} \left(\frac{1}{\text{SSF}_T} + \frac{1}{\text{SSF}_{I_d}} + \frac{1}{av_{\text{EODV}}^{-b}} + \frac{1}{\text{SSF}_{I_c}} + \frac{1}{cv_{\text{EOCV}}^{-d}} \right)$$

where

- CL total cycle life;
- SSF_x single stress factor model of x , where $x = I_d, I_c$, charge and discharge current rates;
- a, b, c , and d curve fit parameters.

b) *Modeling techniques (average SoC):* Other studies have investigated the effect of different starting or average SoC. In [68], three different average SoCs were investigated, 27.5%, 50%, and 72.5%, all cycled with 35% DoD, 4 C. Their results shown in Fig. 17 show an increasing degradation rate for lower SoC, modeled as inversely exponentially dependent on SoC, as follows:

$$b(\text{SoC}) = 0.2943 \exp(-0.01943\text{SoC}). \quad (24)$$

This increasing degradation rate at lower SoC can be explained by the fact that the impedance of the cell increases as the cell is discharged [21], [131], [136]. This results in reduced power capabilities and more self-heating. This is also temperature-dependent, and higher C-rates might aggravate its effect.

In [114], the effect of minimum SoC on various CS cycles for PHEVs was tested on NMC-LMO cells at 30 °C and

25%–45% minimum SoC with varying C-rate. Their results show an exponentially increasing degradation at higher SoCs. Similar results are found in [89] for LFP cells cycled at 1–1.8 °C, 30 °C. In [89] and [114], the calendar aging was not subtracted, which might be a possible explanation for their results. In [107], a very slight increase in aging was observed at higher SoC for cells cycled with a C-rate of 10 C, whereas, for lower temperatures and lower C-rates, the effect of SoC was found negligible. The authors followed an Arrhenius equation, where the degradation was linearly dependent on SoC, as follows:

$$Q_{\text{loss}} = (\alpha \text{SoC} + \beta) \exp \frac{-E_a + \eta I}{R(273.15 + T)} Ah^z. \quad (25)$$

Schmalstieg *et al.* [13] cycled NMC cells with various DoDs at 1 °C, 35 °C, and subtracted the expected calendar aging results from their cycling aging results. The resulting data showed the lowest aging around an average SoC of 50%. Similar results were found in [79] and [81].

c) Modeling limitations and challenges [SoC (cyclic)]:

Concerning the effect of EOCV, a consensus exists that a higher EOCV leads to increased degradation. However, at these high SoC levels, battery chargers charge with a decreasing average current to maintain a CV instead of constant current charging in the majority of the SoC range. Therefore, the effect of EOCV might be attributed primarily to calendar aging mechanisms.

Less consensus on the effect of average SoC on LIB aging is observed partially due to the influence of other parameters, such as temperature, DoD, C-rate, and chemistry, but also due to the other mechanical and kinetic changes inside the cell, such as an increased impedance at lower SoC and volume changes due to the different electrode intercalation compounds [137], [138], as shown in Fig. 10. Gantenbein *et al.* [137] analyzed five NCA cells each cycled with 20% DoD around evenly distributed SoC intervals. The highest degradation was observed for the cells cycled in stage 2 (see Fig. 10).

A similar investigation was done in [43], where 10% DoD cycles are spread out evenly over the entire SoC range. The results are shown in Fig. 18 and are in line with what was found in [137]. Here, the bars show the total degradation per SoC range, whereas the lines show the DVA of both electrodes and the complete cell. However, the results of Fig. 18 oppose their results for cells cycled with a DOD of 50%, which showed the least aging with an average SoC 75%. This shows that SoC and DoD's effects have strong interdependences that are hard to capture in empirical aging models, as the effect will always be different depending on the starting point and cycle depth. Aside from a high interdependence, testing for only a limited amount of time or cycles may also lead to false conclusions on total lifetime, as was demonstrated in [43]. Here, NMC cells were tested around 25%–75% SoC with 1 C at 20 °C. In the first 300 full equivalent cycles (FECs), the most aging was observed at the highest SoC. Nevertheless, the highest cycle lifetime was observed at the highest average SoC as well. Further investigation showed that a more stable SEI is formed at higher cell voltages, whereas the SEI formed

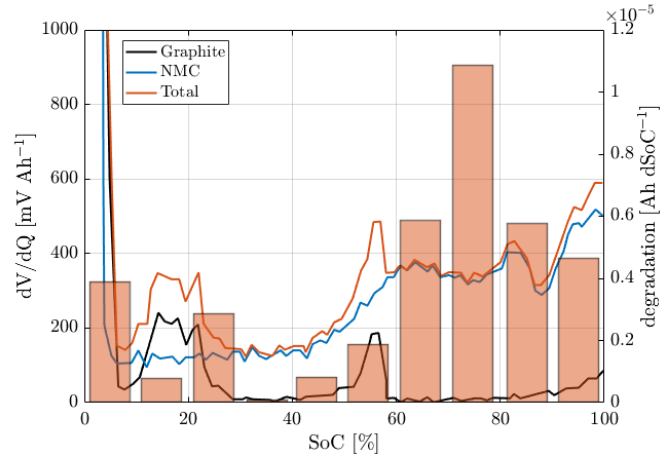


Fig. 18. Left: DVA of an NMC cell and right: the degradation rate of cycles with 10% DoD for ten different SoC intervals. The orange bars illustrate the strong SoC dependence on the effect of DoD. The most degradation is observed at the place where the anode potential is the lowest or where there is a phase transition at the anode. These cells are cycled with 10% DoD, 1 °C, and 45 °C, around ten different SoC regions. Based on data obtained from [43].

at lower cell voltages evolves to be more porous. Especially, the SEI formed in the CV region is said to better protect the anode material from the electrolyte. As a result, longer cycle lives were observed for higher cell voltages.

d) Key insights on SoC (cyclic): The following key insights can be summarized based on the above review.

- 1) A higher EOCV results in increased aging; due to the reduced current rate in the CV region, this is expected to be due to increased calendar aging.
- 2) The effect of SoC is strongly dependent on other operating conditions, such as C-rate, temperature, and DoD. More specifically, cells tested at low C-rates, higher voltages, and higher temperatures are likely to have a significant calendar aging superposition, resulting in less aging at lower SoC. In contrast, cells cycled with higher C-rates or higher DoD appear to be more affected by the lower impedance at lower SoC. Probably having a higher cycle life when cycled around 50% SoC.
- 3) A fast initial decrease in capacity due to high cell voltages does not necessarily have to result in a reduced lifetime, as higher cell voltages may lead to a more stable SEI layer.

7) Depth of Discharge: The final stress factor to be discussed is the DoD, sometimes also called cycle depth.⁶ In this study, DoD is defined as the percentage of extracted charge with respect to the maximum available amount of charge. A usual rule of thumb is that an increasing DoD reduces the cycle lifetime [21], [74], [106]. However, as will be discussed, this is not valid for all reviewed studies. Generally, two different testing approaches exist to determine the detrimental effect of DoD: 1) starting from 100% SoC or 2) cycling

⁶Existing DoD definitions in the literature are contradictory, and at least four conflicting definitions are used, namely, 1) the inverse of the SoC; 2) the energy discharged from the battery compared to 100% SoC; 3) the full cycle consisting of one equal discharging and charging event; or 4) the half-cycle consisting of one charging or discharging event [139].

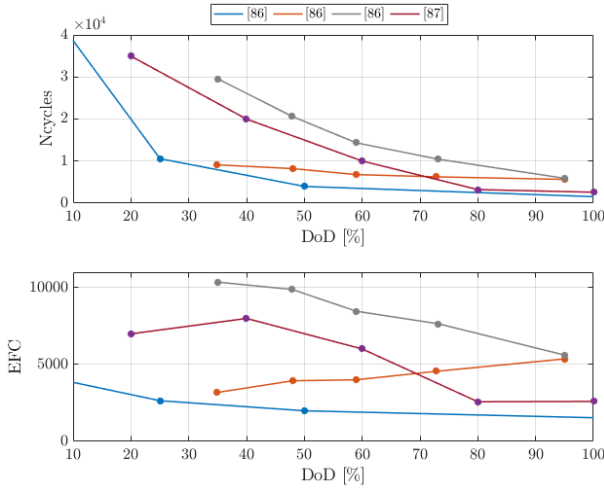


Fig. 19. Comparison of the effect of DoD in two different studies. Top: DoD versus cycles. Bottom: DoD versus FECs. Even though many studies find a good correlation with the Wöhler curve in terms of number of cycles, in terms of total charge throughput, cycle life does not necessarily decrease for higher DoD.

around a mean SoC. Both methods are limited because the starting point of the cycle determines the corresponding effect of DoD, as discussed in Section III-B6. Depending on the application of the model, one of the two methods can be preferred.

a) *Modeling techniques (DoD)*: An often found correlation between DoD and degradation follows the Wöhler curve, also known as the S-N curve or the Palmgren–Miner rule [26]. Originating from mechanical stress in railway engineering, this curve describes an object's lifetime, expressed in terms of the number of cycles (N) and cyclic stress (S) [88]. For LIB degradation, it is frequently used to describe the battery cycle life as a function of DoD. Here, the degradation rate decreases as the DoD increases. Various papers have found good correlation with this dependence [42], [68], [74], [92], [93], [106], [117]. Some of their results are shown in Fig. 19(a) and (b).

When plotted as a function of the number of cycles, a good correlation with the Wöhler curve is observed. However, when plotted as a function of FECs, this behavior is not always seen. Therefore, in terms of total charge throughput, cycle life does not necessarily have to decrease for a higher DoD.

Based on the Wöhler curve, several studies have modeled the degradation to be exponentially dependent on DoD [89], [92], [106]; an example from [106] is shown as follows:

$$\text{CL(DoD)} = ae^{b \cdot \text{DoD}} + ce^{d \cdot \text{DoD}} \quad (26)$$

where

CL(DoD) cycle life as function of DoD;
 a, b, c , and d curve fit parameters.

Others, such as [68], have modeled the DoD dependence using a power-law relationship, as follows:

$$C_{\text{fade}} = 0.0123 \cdot cd^{0.07162} \cdot nc^{0.5} \quad (27)$$

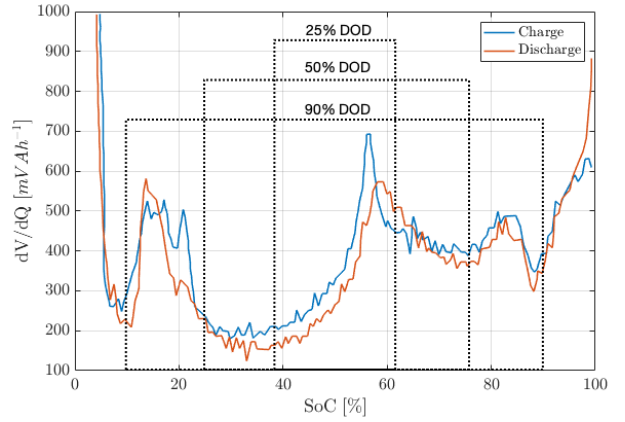


Fig. 20. Differential voltage curve for an NMC cell under slow charge and discharge rates. The number of phase transitions depends on the DoD and the starting SoC, as indicated by the different intervals.

where

C_{fade} percentage capacity fade;
 cd cycle depth/depth of discharge;
 nc number of cycles.

b) *Modeling limitations and challenges (DoD)*: Even though the Wöhler curve has shown a good correlation with aging data in several studies, readers and modelers should be aware that these results are also dependent on other stress factors and, therefore, cannot be generalized or extrapolated to other operating conditions.

In fact, in [81], [88], and [137], it is argued that one of the causes of degradation due to DoD is the traversing between different phases of the anode and the cathode. As a result, the effect of DoD is heavily SoC-dependent. Following this analysis, for a given DoD, it could be possible that the battery stays in the same voltage plateau, resulting in negligible effects between various DoD, or a slight change in SoC might lead to a considerable capacity decrease (or resistance increase), as shown in Figs. 18 and 20. Two observations are made: 1) the most degradation is observed at higher SoC, where the anode is in its second stage according to Fig. 10 and the largest change in anode volume is observed [137] and 2) second, regions where phase transitions occur lead to additional degradation. In [140], it was confirmed for an NMC cell that traversing of the voltage plateaus resulted in more volume changes of the cell, whereas the volume change is low if the cycle stays within a particular plateau region. These volume changes can cause particle cracking, resulting in accelerated growth of the SEI layer [43], [141]. Therefore, Oh *et al.* [140] conclude that the stresses per FEC are dependent on the number of voltage plateaus traversed.

Similar conclusions for NMC cells were drawn in [88], where an increased DoD showed an increased degradation. For all cases resulting in an almost linear course of degradation for both resistance and capacity, DVA showed that cycles that cross anode voltage plateaus caused additional degradation due to mechanical stress. Over time, the voltage peaks decreased. The authors conclude that the disordering of the anode lattice

could be a possible explanation. Another explanation could be an inhomogeneous load over the electrode, as was shown in simulations in [142] and [5]. Overall, the lowest degradation was observed for cells cycled around an average SoC of 50%, probably caused by a strong superposition of other SoC-dependent mechanisms caused by cell voltage or impedance.

A similar linear course of degradation was observed in [42], where the cycle life of batteries for satellite applications was investigated by cycling NCA cells with only one to four cycles per day. The authors noticed that, as the cycling frequency increased, a linear component on top of $\sqrt{\text{time}}$ behavior started to arise. This linear degradation of capacity and resistance increased as the DoD increased. Based on a destructive physical analysis, the authors argued that damage to the cathode's active material reduced lithium adsorption capability. Furthermore, transmission electron microscopy showed that, compared to calendar aging, the amorphous⁷ layer was less thick and consisted of two layers of active material. A linear component as a result of cyclic aging was observed in other studies as well [13], [42], [79], [106], [122]. An example of this is shown in Fig. 12, where an increasing DoD results in an increasing linear degradation. Unfortunately, no further investigation on the root cause of DoD-dependent degradation was performed in [13], [42], [79], [106], and [122].

Due to the complex correlations between SoC and DoD, it is incredibly challenging to model their correlations. To this extend, none of the above described models can accurately model these effects outside the conditions at which these models are tested, which shows the importance of carefully selecting test conditions.

So far, all studies discussed have reported an increase in degradation for higher DOD, given that all other conditions are equal. However, in [43] and [100], a higher DoD actually leads to less aging. In [43], significantly less degradation was observed for cells cycled with 100% DoD compared to other DoDs, independent of C-rate and temperature. Using electrical impedance spectroscopy, the authors discovered that the resistance remained constant for a long time despite a fast initial increase. The cells cycled with a DoD of 50% showed a more linear increase in resistance. As a result, it also reached the critical SEI layer resistance earlier, causing lithium plating and a reduced lifetime. Further investigation showed that the CV region played an important role in forming a stable SEI layer, indicating that its formation is strongly voltage-dependent and kinetically slow. Therefore, the cells cycled at 100% DoD might have a more stable SEI layer resulting in longer cycle life.

The effect of DOD on an LFP cell's cycle life was also tested in [100]. Their results are shown in Figs. 21 and 22. The DoD dependence on cycle life is shown in Fig. 19(b), showing an increased cycle life for a DoD $\geq 50\%$ around an average SoC of 50%, at 1 C at 30 °C. In contrast to some of the studies mentioned above, the authors did not find any clear correlation between the anode staging phenomena and the DoD-dependent degradation. Note that these cells were tested at a starting SoC

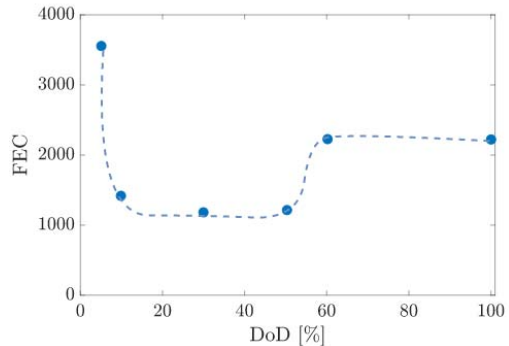


Fig. 21. Number of FECs for different DOD ranges obtained in [100], before reaching 90% remaining capacity. Remarkably, less aging is observed for high DoD cycles. The cells have been cycled with 1 C at 30° around 50% average SoC.

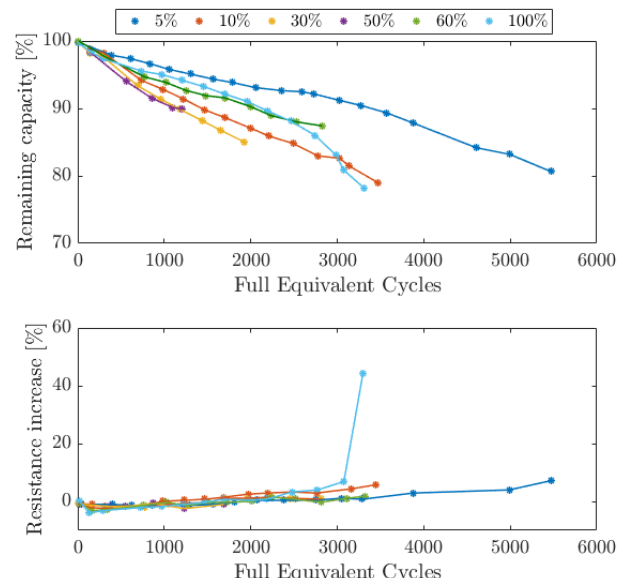


Fig. 22. Degradation of LFP cells cycled with varying DoD, 1 C, and 30°. The results show a reduced degradation for cells cycled with a DoD above 50% [100]. However, the increase in resistance for the cells cycled with 100% DoD around 3000 FEC could indicate the onset of lithium plating and, therefore, significantly reduce its lifetime.

of 100%. Therefore, the reduced degradation at higher DoD's might result from a lower average cell voltage. Also, following the results of [43], it could be argued that a higher average voltage results in the faster but more stable growth of the SEI layer. The total cycle life of these cells could, therefore, be improved in the long term. This is supported by the fact that only the cells cycled at 100% DoD showed an increase in degradation (both capacity and resistance) after 3000 FEC, possibly resulting from electrolyte depletion or lithium plating.

Fig. 22 also shows that the cells with a moderate increase in resistance only experienced low structural damage due to cycling [58]. Another possible explanation for the discrepancy in the results of [100] can be that the lattice structure of LFP cells better allows for complete delithiation compared to NMC cells, resulting from higher stability [143], [144]. Furthermore, manganese-containing chemistries, such as the cells studied

⁷Without a clearly defined shape or form.

in [43], [88], and [140], are more prone to SoC-induced aging. Due to aging mechanisms, such as the Jahn–Teller distortion, transition metal dissolution, structural damage due to complete delithiation, and electrolyte oxidation [2], [21], [49], of course, additional testing and analysis should be carried out to pinpoint the exact cause of degradation.

c) Key insights on the effect of DoD: The following key insights on the effect of DoD on LIB aging can be summarized.

- 1) Most often, the cycle life decreases as DoD increases. However, in terms of total charge throughput, different optima are observed at various DoD's.
- 2) The DoD effect can also be perceived differently due to the coexistence of various aging mechanisms and the interdependence with other stress factors, such as high and low cell voltage, different temperatures, or various current rates. As a result, assessing DoD-dependent degradation can be very difficult, especially for highly varying power profiles.
- 3) The effect of DoD is strongly SoC-dependent. More specifically, the traversing of voltage plateaus, or the transitioning between electrode phases, has increased mechanical stress due to volume changes. Often resulting in a linear component in aging behavior. In addition, the CV region can play a significant role in providing a stable SEI layer and, therefore, affect the degradation due to DoD.

IV. CURRENT CHALLENGES AND FUTURE TRENDS

This section provides an overview of the current challenges and future trends with respect to LIB aging and aging modeling.

A. New Battery Chemistries

For EV and RES applications, two of the most common cathode materials are lithium NMC oxide and LFP [145], with graphite as anode material. The main objective in the development of new chemistries is to improve performance. However, also, the environmental and societal footprint of the raw materials will start to play a more significant role as the LIB market increases. Therefore, the use of rare and toxic elements, such as cobalt and nickel, should be avoided as much as possible [145]–[147]. In the future, some promising new anode materials could be based on LTO, silicon (Si), or Tin (Sn), or other carbon-based structures, such as graphene or carbon nanotubes [146]. The list of future cathode materials is smaller and will probably involve new combinations of the existing materials mentioned in Section II [147]. Another possible improvement could be the use of nanostructures. Besides incremental changes to existing technology, other more disruptive chemistries include Li–air and Li–sulfur, which achieves very high energy densities. Modeling the aging behavior of these new chemistries will play an important role in quantifying their performance. Si-C-based anode materials, for example, provide exceptional energy density at the expense of a significantly reduced lifetime due to structural damage [32]. For more information, interested readers are directed to [32], [146], and [147].

B. Second-Life Batteries

Besides new battery chemistries, another way to reduce the cost and environmental impact of LIBs is to use second-life batteries (SLBs). SLBs are repurposed EV batteries deemed unfit for EV applications but still have sufficient capacity for other stationary applications, such as grid reinforcement. Reusing these batteries lowers the cost of LIBs while also lowering the environmental impact by reducing the demand for raw materials. Martinez-Laserna *et al.* [148] and Neubauer *et al.* [149] showed that first-life battery performance is a critical parameter to assess the remaining value and SoH for second-life applications. As a result, modeling and optimizing battery aging in both first life and second life can reduce the environmental impact of LIBs. However, most of the studies currently only investigate aging behavior in the first part of LIB life. For example, studies that model the aging behavior as a function of $\sqrt{\text{time}}$ or $\sqrt{\text{Ah}}$ tend to miss out on aging effects in the latter part of their life, such as lithium plating, and are, therefore, less or not suitable for second-life applications.

C. Fast Charging

Range anxiety and long charging times are two of the main challenges for EVs at this moment [150]. Fast charging is an effective tool for relieving EV users' range anxiety. Currently, most EVs can withstand maximum charging powers in the range of 50–150 kW. However, new top-end vehicles, such as the Porsche Taycan or Audi e-tron GT, can charge with powers up to 350 kW [151]. These maximum charging rates and total charging time are currently limited by the battery's rate capability and the thermal management of the EV. Naturally, charging at these high rates is far more damaging to the battery, and to mitigate this, more and more EVs have thermally managed battery packs. Therefore, correlating the effects of temperature, C-rate, and DoD is important to accurately calculate the deteriorating effect of fast charging.

D. Thermally Managed Systems

Thermal management is becoming more common as a way to improve the lifetime of LIB systems. Thermal management for fast charging is an example of this. However, thermal management is also used at lower charging rates to prevent lithium plating at low temperatures. Other applications include stationary applications, such as RES integration or ancillary services. These systems generally have climate control systems that control the temperature to be around 20 °C–25 °C to have optimal cycling performance. To this extend, extensive testing of aging behavior around room temperature could be argued to be vital for good modeling accuracy.

E. Artificial Intelligence for Aging Estimation

As mentioned in the introduction, the different aging estimation techniques, such as PBMs, ECMs, or Ems, all provide different tradeoffs between modeling accuracy, complexity, and computational demand. Recently, various AI techniques have been investigated as ways to achieve high accuracy

with low computational demand. These techniques can be differentiated into two groups. The first group trains their AIs on model-fit features, such as internal resistance and SoC, to estimate the SoH. These models then require other models to extract these internal parameters. The second group uses external features, such as open-circuit voltage and incremental capacity curves, to estimate SoH [20]. The latter does not rely on other models to calculate the internal parameters and, therefore, has lower computational complexity, and, as a result, is better suited for real-time applications.

V. CONCLUSION

Due to their critical role in the electrification of transportation and the integration of RESs, lithium-ion batteries are recognized as a key technology in achieving the goals set in the Paris climate agreement. Understanding battery aging is one of the main scientific problems related to LIBs and vital to understand better the tradeoffs between characteristics, such as performance, cost, and lifetime.

In this article, a review of the behavior and empirical modeling of LIB aging was presented, focusing on the effect and interdependence of operational stress factors. The presented review concludes that it is very difficult to generalize aging behavior, with respect to the effect of operational conditions. Usually, the resulting aging is caused by a combination of stress factors rather than attributable to a single stress factor. To this extent, users of empirical and semiempirical battery aging models should be cautious of their models' limitations and the correlations between the stress factors. To summarize some of the key findings, the following is given.

- 1) SEI growth is considered to be the most important aging mechanism for both cycling and calendar aging. A strong correlation with anode potential is observed during idle conditions: a higher SoC results in increased SEI layer growth. However, other kinetic effects during cycling can accelerate aging at low SoC. SoC-dependent calendar aging is often modeled to exponentially dependent, whereas its effect on cyclic aging can have different forms depending on the operating conditions.
- 2) Because of the passivation character of the SEI layer, the aging behavior is most commonly modeled using a t^z or Ah^z relationship, with $0.5 \leq z \leq 1$. Unfortunately, many cyclic aging models do not differentiate between cyclic aging and calendar aging and, therefore, measure their combined effect. Others have subtracted calendar aging from their cyclic aging results to model the effect of cyclic aging only, resulting in higher modeling accuracy.
- 3) The Arrhenius law is an effective model for the temperature dependence of calendar aging. However, during cycling, different aging mechanisms are observed above and below room temperature. These should be considered when modeling cyclic aging below room temperature. Since most studies are based on accelerated test conditions, this is frequently overlooked. Possible solutions include combining positive and negative activation energy in Arrhenius laws or including parabolic temperature dependencies.

- 4) The effect of C-rate is often modeled to be exponentially dependent. Several studies, however, have found insignificant differences at C-rates less than 2. Furthermore, multiple studies have found a strong correlation between C-rate and temperature; as temperature rises, the impact of C-rate decreases significantly. Many models do not take this into account, which is in part due to accelerated testing conditions.
- 5) Several studies modeled the DoD-dependent degradation based on Wohler curves or other exponential curves. However, the effect of DoD is directly related to other SoC-associated mechanisms and is, therefore, probably the most difficult stress factor to model. In addition, the impact of DoD is affected by volume change due to electrode phase transitions and is, thus, also related to C-rate and temperature.

The summation of conclusions is all examples of the challenges involved in modeling LIB aging behavior. Readers and modelers can mitigate these challenges by improving the design of aging tests, aging models, and aging model applications using the knowledge provided in this article. The authors hope that, by doing so, they can help with overcoming the challenges of LIBs.

REFERENCES

- [1] B. L. Ellis, K. T. Lee, and L. F. Nazar, "Positive electrode materials for Li-ion and Li-batteries," *Chem. Mater.*, vol. 22, no. 3, pp. 691–714, Jan. 2010, doi: [10.1021/cm902696](https://doi.org/10.1021/cm902696).
- [2] X. Han *et al.*, "A review on the key issues of the lithium ion battery degradation among the whole life cycle," *eTransportation*, vol. 1, Aug. 2019, Art. no. 100005. [Online]. Available: <https://www.sciencedirect.com/science/article/pii/S2590116819300050>
- [3] I. Tsiropoulos, D. Tarvydas, and N. Lebedeva, "Li-ion batteries for mobility and stationary applications," Joint Res. Centre, Eur. Commission, Brussels, Belgium, Tech. Rep. EUR 29440 EN, OP KJ-NA-29440-EN-N, 2018. [Online]. Available: <https://publications.jrc.ec.europa.eu/repository/handle/JRC113360>
- [4] Y. Zheng *et al.*, "Cell state-of-charge inconsistency estimation for LiFePO₄ battery pack in hybrid electric vehicles using mean-difference model," *Appl. Energy*, vol. 111, pp. 571–580, Nov. 2013. [Online]. Available: <https://www.sciencedirect.com/science/article/pii/S0306261913004601>
- [5] M. Doyle, T. F. Fuller, and J. Newman, "Modeling of galvanostatic charge and discharge of the lithium/polymer/insertion cell," *J. Electrochem. Soc.*, vol. 140, no. 6, pp. 1526–1533, 1993, doi: [10.1149/1.2221597](https://doi.org/10.1149/1.2221597).
- [6] M. Jafari, K. Khan, and L. Gauchia, "Deterministic models of Li-ion battery aging: It is a matter of scale," *J. Energy Storage*, vol. 20, pp. 67–77, Dec. 2018. [Online]. Available: [http://www.sciencedirect.com/science/article/pii/S2352152X18303098](https://www.sciencedirect.com/science/article/pii/S2352152X18303098)
- [7] P. W. C. Northrop, M. Pathak, D. Rife, S. De, S. Santhanagopalan, and V. R. Subramanian, "Efficient simulation and model reformulation of two-dimensional electrochemical thermal behavior of lithium-ion batteries," *J. Electrochem. Soc.*, vol. 162, no. 6, pp. A940–A951, 2015, doi: [10.1149/2.0341506jes](https://doi.org/10.1149/2.0341506jes).
- [8] R. Darling and J. Newman, "Modeling side reactions in composite Li_yMn₂O₄ electrodes," *J. Electrochem. Soc.*, vol. 145, no. 3, pp. 990–998, Mar. 1998, doi: [10.1149/1.1838376](https://doi.org/10.1149/1.1838376).
- [9] P. Ramadass, B. Haran, P. M. Gomadam, R. White, and B. N. Popov, "Development of first principles capacity fade model for Li-ion cells," *J. Electrochem. Soc.*, vol. 151, no. 2, p. A196, 2004, doi: [10.1149/1.1634273](https://doi.org/10.1149/1.1634273).
- [10] J. Christensen and J. Newman, "A mathematical model for the lithium-ion negative electrode solid electrolyte interphase," *J. Electrochem. Soc.*, vol. 151, no. 11, 2004, Art. no. A1977, doi: [10.1149/1.1804812](https://doi.org/10.1149/1.1804812).
- [11] A. V. Randall, R. D. Perkins, X. Zhang, and G. L. Plett, "Controls oriented reduced order modeling of solid-electrolyte interphase layer growth," *J. Power Sources*, vol. 209, pp. 282–288, Jul. 2012. [Online]. Available: <https://www.sciencedirect.com/science/article/pii/S0378775312005368>

- [12] A. Barré, B. Deguilhem, S. Grolleau, M. Gérard, F. Suard, and D. Riu, "A review on lithium-ion battery ageing mechanisms and estimations for automotive applications," *J. Power Sources*, vol. 241, pp. 680–689, Nov. 2013. [Online]. Available: <https://www.sciencedirect.com/science/article/pii/S0378775313008185>
- [13] J. Schmalstieg, S. Käbitz, M. Ecker, and D. U. Sauer, "A holistic aging model for Li(NiMnCo)O₂ based 18650 lithium-ion batteries," *J. Power Sources*, vol. 257, pp. 325–334, Jul. 2014. [Online]. Available: <https://www.sciencedirect.com/science/article/pii/S0378775314001876>
- [14] S. Nejad, D. T. Gladwin, and D. A. Stone, "A systematic review of lumped-parameter equivalent circuit models for real-time estimation of lithium-ion battery states," *J. Power Sources*, vol. 316, pp. 183–196, Jun. 2016. [Online]. Available: <https://www.sciencedirect.com/science/article/pii/S0378775316302427>
- [15] Z. Wang, J. Ma, L. Zhang, "State-of-health estimation for lithium-ion batteries based on the multi-island genetic algorithm and the Gaussian process regression," *IEEE Access*, vol. 5, pp. 21286–21295, 2017.
- [16] M. Berecibar *et al.*, "Online state of health estimation on NMC cells based on predictive analytics," *J. Power Sources*, vol. 320, pp. 239–250, Jul. 2016. [Online]. Available: <https://www.sciencedirect.com/science/article/pii/S0378775316304827>
- [17] H. Pan, Z. Lü, H. Wang, H. Wei, and L. Chen, "Novel battery state-of-health online estimation method using multiple health indicators and an extreme learning machine," *Energy*, vol. 160, pp. 466–477, Oct. 2018. [Online]. Available: <https://www.sciencedirect.com/science/article/pii/S0360544218312854>
- [18] D. Yang, Y. Wang, R. Pan, R. Chen, and Z. Chen, "State-of-health estimation for the lithium-ion battery based on support vector regression," *Appl. Energy*, vol. 227, pp. 273–283, Oct. 2018. [Online]. Available: <https://www.sciencedirect.com/science/article/pii/S0306261917311169>
- [19] K. Liu, X. Hu, Z. Wei, Y. Li, and Y. Jiang, "Modified Gaussian process regression models for cyclic capacity prediction of lithium-ion batteries," *IEEE Trans. Transport. Electricific.*, vol. 5, no. 4, pp. 1225–1236, Dec. 2019.
- [20] Y. Li *et al.*, "Data-driven health estimation and lifetime prediction of lithium-ion batteries: A review," *Renew. Sustain. Energy Rev.*, vol. 113, Oct. 2019, Art. no. 109254. [Online]. Available: <https://www.sciencedirect.com/science/article/pii/S136403211930454X>
- [21] J. Vetter *et al.*, "Ageing mechanisms in lithium-ion batteries," *J. Power Sources*, vol. 147, nos. 1–2, pp. 269–281, 2005. [Online]. Available: <https://www.sciencedirect.com/science/article/pii/S0378775305000832>
- [22] M. Broussely *et al.*, "Main aging mechanisms in Li-ion batteries," *J. Power Sources*, vol. 146, nos. 1–2, pp. 90–96, 2005. [Online]. Available: <http://www.sciencedirect.com/science/article/pii/S0378775305005082>
- [23] X. Han *et al.*, "A review on the key issues of the lithium ion battery degradation among the whole life cycle," *eTransportation*, vol. 1, Aug. 2019, Art. no. 100005. [Online]. Available: <http://www.sciencedirect.com/science/article/pii/S2590116819300050>
- [24] X. Han, M. Ouyang, L. Lu, J. Li, Y. Zheng, and Z. Li, "A comparative study of commercial lithium ion battery cycle life in electrical vehicle: Aging mechanism identification," *J. Power Sources*, vol. 251, pp. 38–54, Apr. 2014.
- [25] M. Scarfogliero *et al.*, "Lithium-ion batteries for electric vehicles: A review on aging models for vehicle-to-grid services," in *Proc. Int. Conf. Electr. Electron. Technol. Automot.*, Jul. 2018, pp. 1–6.
- [26] A. Ahmadian, M. Sedghi, A. Elkamel, M. Fowler, and M. A. Golkar, "Plug-in electric vehicle batteries degradation modeling for smart grid studies: Review, assessment and conceptual framework," *Renew. Sustain. Energy Rev.*, vol. 81, pp. 2609–2624, Jan. 2017. [Online]. Available: <http://www.sciencedirect.com/science/article/pii/S1364032117310067>
- [27] R. Xiong, L. Li, and J. Tian, "Towards a smarter battery management system: A critical review on battery state of health monitoring methods," *J. Power Sources*, vol. 405, pp. 18–29, Nov. 2018.
- [28] M. Berecibar, I. Gandiaga, I. Villarreal, N. Omar, J. Van Mierlo, and P. Van den Bossche, "Critical review of state of health estimation methods of Li-ion batteries for real applications," *Renew. Sustain. Energy Rev.*, vol. 56, pp. 572–587, Apr. 2016. [Online]. Available: <http://www.sciencedirect.com/science/article/pii/S1364032115013076>
- [29] M. Lucu, E. Martinez-Laserna, I. Gandiaga, and H. Cambelong, "A critical review on self-adaptive Li-ion battery ageing models," *J. Power Sources*, vol. 401, pp. 85–101, Oct. 2018. [Online]. Available: <http://www.sciencedirect.com/science/article/pii/S0378775318309297>
- [30] M. H. Lipu *et al.*, "A review of state of health and remaining useful life estimation methods for lithium-ion battery in electric vehicles: Challenges and recommendations," *J. Cleaner Prod.*, vol. 205, pp. 115–133, Dec. 2018. [Online]. Available: <http://www.sciencedirect.com/science/article/pii/S0959652618327793>
- [31] C. R. Birkl, M. R. Roberts, E. McTurk, P. G. Bruce, and D. A. Howey, "Degradation diagnostics for lithium ion cells," *J. Power Sources*, vol. 341, pp. 373–386, Feb. 2017. [Online]. Available: <https://www.sciencedirect.com/science/article/pii/S0378775316316998>
- [32] K. Kalaga, M.-T.-F. Rodrigues, S. E. Trask, I. A. Shkrob, and D. P. Abraham, "Calendar-life versus cycle-life aging of lithium-ion cells with silicon-graphite composite electrodes," *Electrochim. Acta*, vol. 280, pp. 221–228, Aug. 2018. [Online]. Available: <https://www.sciencedirect.com/science/article/pii/S0013468618311344>
- [33] C. Pastor-Fernández, T. F. Yu, W. D. Widanage, and J. Marco, "Critical review of non-invasive diagnosis techniques for quantification of degradation modes in lithium-ion batteries," *Renew. Sustain. Energy Rev.*, vol. 109, pp. 138–159, Jul. 2019. [Online]. Available: <https://www.sciencedirect.com/science/article/pii/S136403211930200X>
- [34] E. Sarasketa-Zabala, F. Aguesse, I. Villarreal, L. M. Rodriguez-Martinez, C. M. López, and P. Kubiak, "Understanding lithium inventory loss and sudden performance fade in cylindrical cells during cycling with deep-discharge steps," *J. Phys. Chem. C*, vol. 119, no. 2, pp. 896–906, Jan. 2015.
- [35] C. Delacourt and M. Safari, *Mathematical Modeling of Aging of Li-Ion Batteries*. London, U.K.: Springer, 2016, pp. 151–190, doi: [10.1007/978-1-4471-5677-2_5](https://doi.org/10.1007/978-1-4471-5677-2_5).
- [36] P. Keil *et al.*, "Calendar aging of lithium-ion batteries," *J. Electrochem. Soc.*, vol. 163, no. 9, pp. A1872–A1880, 2016, doi: [10.1149/2.0411609jes](https://doi.org/10.1149/2.0411609jes).
- [37] P. Arora, R. E. White, and M. Doyle, "Capacity fade mechanisms and side reactions in lithium-ion batteries," *J. Electrochem. Soc.*, vol. 145, no. 10, pp. 3647–3667, Oct. 1998, doi: [10.1149/1.1838857](https://doi.org/10.1149/1.1838857).
- [38] J. Park, W. A. Appiah, S. Byun, D. Jin, M.-H. Ryoo, and Y. M. Lee, "Semi-empirical long-term cycle life model coupled with an electrolyte depletion function for large-format graphite/LiFePO₄ lithium-ion batteries," *J. Power Sources*, vol. 365, pp. 257–265, Oct. 2017. [Online]. Available: <https://www.sciencedirect.com/science/article/pii/S0378775317311278>
- [39] B. Xu, A. Oudalov, A. Ulbig, G. Andersson, and D. S. Kirschen, "Modeling of lithium-ion battery degradation for cell life assessment," *IEEE Trans. Smart Grid*, vol. 9, no. 2, pp. 1131–1140, Mar. 2018.
- [40] B. Scrosati and J. Garche, "Lithium batteries: Status, prospects and future," *J. Power Sources*, vol. 195, no. 9, pp. 2419–2430, May 2010. [Online]. Available: <https://www.sciencedirect.com/science/article/pii/S0378775309020564>
- [41] E. Peled, D. B. Tow, A. Merson, A. Gladkich, L. Burstein, and D. Golodnitsky, "Composition, depth profiles and lateral distribution of materials in the SEI built on HOPG-TOF SIMS and XPS studies," *J. Power Sources*, vols. 97–98, pp. 52–57, Jul. 2001. [Online]. Available: <https://www.sciencedirect.com/science/article/pii/S0378775301005055>
- [42] J. Hall, T. Lin, G. Brown, P. Biensan, and F. Bonhomme, "Decay processes and life predictions for lithium ion satellite cells," in *Proc. 4th Int. Energy Convers. Eng. Conf. Exhib. (IECEC)*, Jun. 2006, p. 4078.
- [43] A. Maheshwari, "Modelling, aging and optimal operation of lithium-ion batteries," Ph.D. dissertation, Dept. Elect. Eng., Proefschrift, Amsterdam, The Netherlands, Oct. 2018.
- [44] N. Lin *et al.*, "Understanding the crack formation of graphite particles in cycled commercial lithium-ion batteries by focused ion beam-scanning electron microscopy," *J. Power Sources*, vol. 365, pp. 235–239, Oct. 2017. [Online]. Available: <https://www.sciencedirect.com/science/article/pii/S0378775317310698>
- [45] M. Koltypin, Y. S. Cohen, B. Markovsky, Y. Cohen, and D. Aurbach, "The study of lithium insertion-deinsertion processes into composite graphite electrodes by *in situ* atomic force microscopy (AFM)," *Electrochim. Commun.*, vol. 4, no. 1, pp. 17–23, Jan. 2002. [Online]. Available: <https://www.sciencedirect.com/science/article/pii/S1388248101002648>
- [46] H. Ekstrom. (2019). *Electrode Balancing of a Lithium-Ion Battery With Comsol*. [Online]. Available: <https://www.comsol.com/blogs/electrode-balancing-of-a-lithium-ion-battery-with-comsol/>
- [47] H. J. Ploehn, P. Ramadass, and R. E. White, "Solvent diffusion model for aging of lithium-ion battery cells," *J. Electrochem. Soc.*, vol. 151, no. 3, p. A456, 2004, doi: [10.1149/1.1644601](https://doi.org/10.1149/1.1644601).

- [48] M. Ecker *et al.*, "Development of a lifetime prediction model for lithium-ion batteries based on extended accelerated aging test data," *J. Power Sources*, vol. 215, pp. 248–257, Oct. 2012. [Online]. Available: <https://www.sciencedirect.com/science/article/pii/S0378775312008671>
- [49] M. Wohlfahrt-Mehrens, C. Vogler, and J. Garche, "Aging mechanisms of lithium cathode materials," *J. Power Sources*, vol. 127, nos. 1–2, pp. 58–64, Mar. 2004. [Online]. Available: <https://www.sciencedirect.com/science/article/pii/S0378775303009376>
- [50] X. Liao *et al.*, "Understanding self-discharge mechanism of layered nickel cobalt manganese oxide at high potential," *J. Power Sources*, vol. 286, pp. 551–556, Jul. 2015. [Online]. Available: <https://www.sciencedirect.com/science/article/pii/S0378775315006710>
- [51] T. Joshi, K. Eom, G. Yushin, and T. F. Fuller, "Effects of dissolved transition metals on the electrochemical performance and SEI growth in lithium-ion batteries," *J. Electrochem. Soc.*, vol. 161, no. 12, pp. A1915–A1921, 2014, doi: [10.1149/2.0861412jes](https://doi.org/10.1149/2.0861412jes).
- [52] W. Li, "Review—An unpredictable hazard in lithium-ion batteries from transition metal ions: Dissolution from cathodes, deposition on anodes and elimination strategies," *J. Electrochem. Soc.*, vol. 167, no. 9, Apr. 2020, Art. no. 090514, doi: [10.1149/1945-7111/ab847f](https://doi.org/10.1149/1945-7111/ab847f).
- [53] T.-F. Yi, L.-J. Jiang, J. Shu, C.-B. Yue, R.-S. Zhu, and H.-B. Qiao, "Recent development and application of $\text{Li}_4\text{Ti}_5\text{O}_{12}$ as anode material of lithium ion battery," *J. Phys. Chem. Solids*, vol. 71, no. 9, pp. 1236–1242, Sep. 2010. [Online]. Available: <https://www.sciencedirect.com/science/article/pii/S0022369710001526>
- [54] W. Lu, J. Liu, Y. K. Sun, and K. Amine, "Electrochemical performance of $\text{Li}_{4/3}\text{Ti}_{5/3}\text{O}_4/\text{Li}_{1+x}(\text{Ni}_{1/3}\text{Co}_{1/3}\text{Mn}_{1/3})_{1-x}\text{O}_2$ cell for high power applications," *J. Power Sources*, vol. 167, no. 1, pp. 212–216, May 2007. [Online]. Available: <https://www.sciencedirect.com/science/article/pii/S0378775307000985>
- [55] B. Priyono, P. W. Winowatan, A. Z. Syahrial, Faizah, and A. Subhan, "Optimizing the performance of $\text{Li}_4\text{Ti}_5\text{O}_{12}/\text{LTO}$ by addition of silicon microparticle in half cell lithium-ion battery anode," *IOP Conf. Ser., Earth Environ. Sci.*, vol. 105, Jan. 2018, Art. no. 012121, doi: [10.1088/1755-1315/105/1/012121](https://doi.org/10.1088/1755-1315/105/1/012121).
- [56] C. Zhan, T. Wu, J. Lu, and K. Amine, "Dissolution, migration, and deposition of transition metal ions in Li-ion batteries exemplified by Mn-based cathodes—A critical review," *Energy Environ. Sci.*, vol. 11, no. 2, pp. 243–257, 2018, doi: [10.1039/C7EE03122J](https://doi.org/10.1039/C7EE03122J).
- [57] S. Bourlot, P. Blanchard, and S. Robert, "Investigation of aging mechanisms of high power Li-ion cells used for hybrid electric vehicles," *J. Power Sources*, vol. 196, no. 16, pp. 6841–6846, 2011. [Online]. Available: <https://www.sciencedirect.com/science/article/pii/S0378775310017106>
- [58] M. Kassem, J. Bernard, R. Revel, S. Pélassier, F. Duclaud, and C. Delacourt, "Calendar aging of a graphite/LiFePO₄ cell," *J. Power Sources*, vol. 208, pp. 296–305, Jun. 2012. [Online]. Available: <https://www.sciencedirect.com/science/article/pii/S0378775312004284>
- [59] K. Edström, T. Gustafsson, and J. Thomas, "The cathode-electrolyte interface in the Li-ion battery," *Electrochim. Acta*, vol. 50, no. 2, pp. 397–403, 2004. [Online]. Available: <https://www.sciencedirect.com/science/article/pii/S0013468604006486>
- [60] K. Amine *et al.*, "Advanced cathode materials for high-power applications," *J. Power Sources*, vol. 146, nos. 1–2, pp. 111–115, Aug. 2005. [Online]. Available: <https://www.sciencedirect.com/science/article/pii/S0378775305005173>
- [61] D. Aurbach *et al.*, "The study of surface phenomena related to electrochemical lithium intercalation into Li_xMO_y host materials ($M = \text{Ni}, \text{Mn}$)," *J. Electrochem. Soc.*, vol. 147, no. 4, p. 1322, 2000, doi: [10.1149/1.1393357](https://doi.org/10.1149/1.1393357).
- [62] C. Love, A. Korovina, C. Patridge, K. Swider-Lyons, M. Twigg, and D. Ramaker, "Review of lifepo₄ phase transition mechanisms and new observations from X-ray absorption spectroscopy," *J. Electrochem. Soc.*, vol. 160, pp. A3153–A3161, Jan. 2013.
- [63] K. Y. Chung and K.-B. Kim, "Investigations into capacity fading as a result of a Jahn-Teller distortion in 4 V LiMn_2O_4 thin film electrodes," *Electrochim. Acta*, vol. 49, no. 20, pp. 3327–3337, Aug. 2004. [Online]. Available: <https://www.sciencedirect.com/science/article/pii/S0013468604002865>
- [64] X. Li, Y. Xu, and C. Wang, "Suppression of Jahn-Teller distortion of spinel LiMn_2O_4 cathode," *J. Alloys Compounds*, vol. 479, nos. 1–2, pp. 310–313, Jun. 2009. [Online]. Available: <https://www.sciencedirect.com/science/article/pii/S0925838808022391>
- [65] M. Lewerenz, J. Münnix, J. Schmalstieg, S. Käbitz, M. Knips, and D. U. Sauer, "Systematic aging of commercial LiFePO₄ [Graphite cylindrical cells including a theory explaining rise of capacity during aging]," *J. Power Sources*, vol. 345, pp. 254–263, Mar. 2017. [Online]. Available: <https://www.sciencedirect.com/science/article/pii/S037877531730143X>
- [66] M. Lewerenz, G. Fuchs, L. Becker, and D. U. Sauer, "Irreversible calendar aging and quantification of the reversible capacity loss caused by anode overhang," *J. Energy Storage*, vol. 18, pp. 149–159, Aug. 2018. [Online]. Available: <https://www.sciencedirect.com/science/article/pii/S2352152X18301191>
- [67] E. Redondo-Iglesias, P. Venet, and S. Pelissier, "Eyring acceleration model for predicting calendar ageing of lithium-ion batteries," *J. Energy Storage*, vol. 13, pp. 176–183, Oct. 2017. [Online]. Available: <https://www.sciencedirect.com/science/article/pii/S2352152X17300634>
- [68] D. Stroe, "Lifetime models for lithium-ion batteries used in virtual power plant applications," Ph.D. dissertation, AAU-Energy, Aalborg Univ., Aalborg, Denmark, Nov. 2014.
- [69] S. Grolleau *et al.*, "Calendar aging of commercial graphite/LiFePO₄ cell—Predicting capacity fade under time dependent storage conditions," *J. Power Sources*, vol. 255, pp. 450–458, Jun. 2014. [Online]. Available: <https://www.sciencedirect.com/science/article/pii/S0378775313019411>
- [70] E. Sarasaka-Zabala, I. Gandiaga, L. M. Rodriguez-Martinez, and I. Villarreal, "Calendar ageing analysis of a LiFePO₄/graphite cell with dynamic model validations: Towards realistic lifetime predictions," *J. Power Sources*, vol. 272, pp. 45–57, Dec. 2014. [Online]. Available: <https://www.sciencedirect.com/science/article/pii/S0378775314013068>
- [71] Y. Zheng *et al.*, "Effects of state of charge on the degradation of LiFePO₄/graphite batteries during accelerated storage test," *J. Alloys Compounds*, vol. 639, pp. 406–414, Aug. 2015. [Online]. Available: <https://www.sciencedirect.com/science/article/pii/S0925838815008944>
- [72] D.-I. Stroe, M. Swierczynski, S. K. Kar, and R. Teodorescu, "Degradation behavior of lithium-ion batteries during calendar ageing—The case of the internal resistance increase," *IEEE Trans. Ind. Appl.*, vol. 54, no. 1, pp. 517–525, Jan. 2018.
- [73] I. Bloom *et al.*, "An accelerated calendar and cycle life study of Li-ion cells," *J. Power Sources*, vol. 101, no. 2, pp. 238–247, 2001. [Online]. Available: <https://www.sciencedirect.com/science/article/pii/S0378775301007832>
- [74] M. Swierczynski, D.-I. Stroe, A.-I. Stan, R. Teodorescu, and S. K. Kaer, "Lifetime estimation of the nanoposphate LiFePO₄/C battery chemistry used in fully electric vehicles," *IEEE Trans. Ind. Appl.*, vol. 51, no. 4, pp. 3453–3461, Jul. 2015.
- [75] A. Eddahech, O. Briat, and J.-M. Vinassa, "Performance comparison of four lithium-ion battery technologies under calendar aging," *Energy*, vol. 84, pp. 542–550, May 2015. [Online]. Available: <https://www.sciencedirect.com/science/article/pii/S0360544215003138>
- [76] P. Röder, B. Stiasny, J. C. Ziegler, N. Baba, P. Lagaly, and H.-D. Wiemhöfer, "The impact of calendar aging on the thermal stability of a $\text{LiMn}_2\text{O}_4\text{-Li}(\text{Ni}_{1/3}\text{Mn}_{1/3}\text{Co}_{1/3})\text{O}_2$ /graphite lithium-ion cell," *J. Power Sources*, vol. 268, pp. 315–325, Dec. 2014. [Online]. Available: <https://www.sciencedirect.com/science/article/pii/S0378775314008945>
- [77] J. Belt, V. Utgikar, and I. Bloom, "Calendar and PHEV cycle life aging of high-energy, lithium-ion cells containing blended spinel and layered-oxide cathodes," *J. Power Sources*, vol. 196, no. 23, pp. 10213–10221, Dec. 2011. [Online]. Available: <https://www.sciencedirect.com/science/article/pii/S0378775311016107>
- [78] J. Schmitt, A. Maheshwari, M. Heck, S. Lux, and M. Vetter, "Impedance change and capacity fade of lithium nickel manganese cobalt oxide-based batteries during calendar aging," *J. Power Sources*, vol. 353, pp. 183–194, Jun. 2017. [Online]. Available: <https://www.sciencedirect.com/science/article/pii/S037877531730397X>
- [79] J. de Hoog *et al.*, "Combined cycling and calendar capacity fade modeling of a Nickel-manganese-cobalt oxide cell with real-life profile validation," *Appl. Energy*, vol. 200, pp. 47–61, Aug. 2017. [Online]. Available: <https://www.sciencedirect.com/science/article/pii/S0306261917305251>
- [80] J. Wang *et al.*, "Degradation of lithium ion batteries employing graphite negatives and nickel-cobalt-manganese oxide + spinel manganese oxide positives: Part 1, aging mechanisms and life estimation," *J. Power Sources*, vol. 269, pp. 937–948, Dec. 2014.
- [81] I. Baghdadi, O. Briat, J.-Y. Delétage, P. Gyan, and J.-M. Vinassa, "Lithium battery aging model based on Dakin's degradation approach," *J. Power Sources*, vol. 325, pp. 273–285, Sep. 2016. [Online]. Available: <https://www.sciencedirect.com/science/article/pii/S0378775316307388>

- [82] E. V. Thomas, I. Bloom, J. P. Christoffersen, and V. S. Battaglia, "Statistical methodology for predicting the life of lithium-ion cells via accelerated degradation testing," *J. Power Sources*, vol. 184, no. 1, pp. 312–317, Sep. 2008. [Online]. Available: <https://www.sciencedirect.com/science/article/pii/S0378775308012032>
- [83] E. Redondo-Iglesias, P. Venet, and S. Pelissier, "Influence of the non-conservation of SoC value during calendar ageing tests on modelling the capacity loss of batteries," in *Proc. 10th Int. Conf. Ecol. Vehicles Renew. Energies (EVER)*, Mar. 2015, pp. 1–5.
- [84] H. Yoshida, N. Imamura, T. Inoue, K. Takeda, and H. Naito, "Verification of life estimation model for space lithium-ion cells," *Electrochemistry*, vol. 78, no. 5, pp. 482–488, 2010.
- [85] S. Buller, "Impedance based simulation models for energy storage devices in advanced automotive power systems," Ph.D. dissertation, Inst. Power Electron. Electr. Drives, RWTH Aachen Univ., Aachen, Germany, 2003. [Online]. Available: <https://publications.rwth-aachen.de/record/58812>
- [86] D. Andre, M. Meiler, K. Steiner, H. Walz, T. Soczka-Guth, and D. U. Sauer, "Characterization of high-power lithium-ion batteries by electrochemical impedance spectroscopy. II: Modelling," *J. Power Sources*, vol. 196, no. 12, pp. 5349–5356, Jun. 2011.
- [87] S. Käbitz *et al.*, "Cycle and calendar life study of a graphite|LiNi_{1/3}Mn_{1/3}Co_{1/3}O₂ Li-ion high energy system—Part A: Full cell characterization," *J. Power Sources*, vol. 239, pp. 572–583, Oct. 2013. [Online]. Available: <https://www.sciencedirect.com/science/article/pii/S0378775313004369>
- [88] M. Ecker *et al.*, "Calendar and cycle life study of Li(NiMnCo)O₂-based 18650 lithium-ion batteries," *J. Power Sources*, vol. 248, pp. 839–851, Feb. 2014. [Online]. Available: <https://www.sciencedirect.com/science/article/pii/S03787753130016510>
- [89] L. Lam and P. Bauer, "Practical capacity fading model for Li-ion battery cells in electric vehicles," *IEEE Trans. Power Electron.*, vol. 28, no. 12, pp. 5910–5918, Dec. 2013.
- [90] M. Reichert *et al.*, "Influence of relaxation time on the lifetime of commercial lithium-ion cells," *J. Power Sources*, vol. 239, pp. 45–53, Oct. 2013. [Online]. Available: <https://www.sciencedirect.com/science/article/pii/S0378775313004448>
- [91] M. Ecker, J. B. Gerschler, J. Vogel, S. Käbitz, F. Hust, P. Dechant, and D. U. Sauer, "Development of a lifetime prediction model for lithium-ion batteries based on extended accelerated aging test data," *J. Power Sources*, vol. 215, pp. 248–257, Oct. 2012. [Online]. Available: <https://www.sciencedirect.com/science/article/pii/S0378775312008671>
- [92] A. Millner, "Modeling lithium ion battery degradation in electric vehicles," in *Proc. IEEE Conf. Innov. Technol. Efficient Reliable Electr. Supply*, Sep. 2010, pp. 349–356.
- [93] C. Guenther, B. Schott, W. Hennings, P. Waldowski, and M. A. Danzer, "Model-based investigation of electric vehicle battery aging by means of vehicle-to-grid scenario simulations," *J. Power Sources*, vol. 239, pp. 604–610, Oct. 2013. [Online]. Available: <https://www.sciencedirect.com/science/article/pii/S0378775313003066>
- [94] R. B. Wright *et al.*, "Calendar- and cycle-life studies of advanced technology development program generation 1 lithium-ion batteries," *J. Power Sources*, vol. 110, no. 2, pp. 445–470, Jul. 2002. [Online]. Available: <https://www.sciencedirect.com/science/article/pii/S0378775302002100>
- [95] S. K. Rechekemmer, X. Zang, W. Zhang, and O. Sawodny, "Empirical Li-ion aging model derived from single particle model," *J. Energy Storage*, vol. 21, pp. 773–786, Feb. 2019. [Online]. Available: <https://www.sciencedirect.com/science/article/pii/S2352152X18307588>
- [96] M. Petit, E. Prada, and V. Sauvant-Moynot, "Development of an empirical aging model for Li-ion batteries and application to assess the impact of vehicle-to-grid strategies on battery lifetime," *Appl. Energy*, vol. 172, pp. 398–407, Jun. 2016. [Online]. Available: <https://www.sciencedirect.com/science/article/pii/S0306261916304500>
- [97] V. A. Sethuraman, L. J. Hardwick, V. Srinivasan, and R. Kostecki, "Surface structural disordering in graphite upon lithium intercalation/deintercalation," *J. Power Sources*, vol. 195, no. 11, pp. 3655–3660, Jun. 2010. [Online]. Available: <http://www.sciencedirect.com/science/article/pii/S0378775309022964>
- [98] W.-S. Yoon, K. Y. Chung, J. McBreen, and X.-Q. Yang, "A comparative study on structural changes of LiCo_{1/3}Ni_{1/3}Mn_{1/3}O₂ and LiNi_{0.8}Co_{0.15}Al_{0.05}O₂ during first charge using *in situ* XRD," *Electrochim. Commun.*, vol. 8, no. 8, pp. 1257–1262, Aug. 2006. [Online]. Available: <https://www.sciencedirect.com/science/article/pii/S138824810600227X>
- [99] D. Manka and E. Ivers-Tiffée, "Electro-optical measurements of lithium intercalation/de-intercalation at graphite anode surfaces," *Electrochim. Acta*, vol. 186, pp. 642–653, Dec. 2015. [Online]. Available: <https://www.sciencedirect.com/science/article/pii/S0013468615306538>
- [100] E. Sarasketa-Zabala, I. Gandiaga, E. Martinez-Laserna, L. M. Rodriguez-Martinez, and I. Villarreal, "Cycle ageing analysis of a LiFePO₄/graphite cell with dynamic model validations: Towards realistic lifetime predictions," *J. Power Sources*, vol. 275, pp. 573–587, Feb. 2015. [Online]. Available: <https://www.sciencedirect.com/science/article/pii/S0378775314017728>
- [101] A. Marongiu, M. Roscher, and D. U. Sauer, "Influence of the vehicle-to-grid strategy on the aging behavior of lithium battery electric vehicles," *Appl. Energy*, vol. 137, pp. 899–912, Jan. 2015. [Online]. Available: <https://www.sciencedirect.com/science/article/pii/S030626191400645X>
- [102] R. Dufo-López and J. L. Bernal-Agustín, "Multi-objective design of PV-wind-diesel-hydrogen-battery systems," *Renew. Energy*, vol. 33, no. 12, pp. 2559–2572, Dec. 2008. [Online]. Available: <https://www.sciencedirect.com/science/article/pii/S0960148108000724>
- [103] S. Mishra, M. Pecht, T. Smith, I. McNee, and R. Harris, "Remaining life prediction of electronic products using life consumption monitoring approach," Univ. Maryland, MD, USA, Jan. 2002.
- [104] Y.-L. Lee and T. Tjhung, "Rainflow cycle counting techniques," in *Metal Fatigue Analysis Handbook*, Y.-L. Lee, M. E. Barkey, and H.-T. Kang, Eds. Boston, MA, USA: Butterworth-Heinemann, 2012, pp. 89–114. [Online]. Available: <https://www.sciencedirect.com/science/article/pii/B9780123852045000033>
- [105] J. Wang *et al.*, "Cycle-life model for graphite-LiFePO₄ cells," *J. Power Sources*, vol. 196, no. 8, pp. 3942–3948, Apr. 2011. [Online]. Available: <https://www.sciencedirect.com/science/article/pii/S0378775310021269>
- [106] N. Omar *et al.*, "Lithium iron phosphate based battery—Assessment of the aging parameters and development of cycle life model," *Appl. Energy*, vol. 113, pp. 1575–1585, Jan. 2014.
- [107] G. Suri and S. Onori, "A control-oriented cycle-life model for hybrid electric vehicle lithium-ion batteries," *Energy*, vol. 96, pp. 644–653, Feb. 2016. [Online]. Available: <https://www.sciencedirect.com/science/article/pii/S0360544215016382>
- [108] Z. Li, L. Lu, M. Ouyang, and Y. Xiao, "Modeling the capacity degradation of LiFePO₄/graphite batteries based on stress coupling analysis," *J. Power Sources*, vol. 196, no. 22, pp. 9757–9766, Nov. 2011.
- [109] F. Todeschini, S. Onori, and G. Rizzoni, "An experimentally validated capacity degradation model for Li-ion batteries in PHEVs applications," *IFAC Proc. Vols.*, vol. 45, no. 20, pp. 456–461, 2012. [Online]. Available: <https://www.sciencedirect.com/science/article/pii/S1474667016347966>
- [110] M. L. Bacci, F. Cheli, E. Sabbioni, D. Tarsitano, and M. Vignati, "Aging models for high capacity LiFePO₄ cells," in *Proc. Int. Conf. Electr. Electron. Technol. Automot.*, Jun. 2017, pp. 1–6.
- [111] M. Ebrahimi, M. Rastegar, M. Mohammadi, A. Palomino, and M. Parvania, "Stochastic charging optimization of V2G-capable PEVs: A comprehensive model for battery aging and customer service quality," *IEEE Trans. Transport. Electrific.*, vol. 6, no. 3, pp. 1026–1034, Sep. 2020.
- [112] M. Schimpf, M. E. von Kuepach, M. Naumann, H. C. Hesse, K. Smith, and A. Jossen, "Comprehensive modeling of temperature-dependent degradation mechanisms in lithium iron phosphate batteries," *J. Electrochim. Soc.*, vol. 165, no. 2, pp. A181–A193, 2018, doi: [10.1149/2.1181714jes](https://doi.org/10.1149/2.1181714jes).
- [113] M. Ouyang, X. Feng, X. Han, L. Lu, Z. Li, and X. He, "A dynamic capacity degradation model and its applications considering varying load for a large format Li-ion battery," *Appl. Energy*, vol. 165, pp. 48–59, Mar. 2016. [Online]. Available: <https://www.sciencedirect.com/science/article/pii/S0306261915016360>
- [114] A. Cordoba-Arenas, S. Onori, Y. Guezenec, and G. Rizzoni, "Capacity and power fade cycle-life model for plug-in hybrid electric vehicle lithium-ion battery cells containing blended spinel and layered-oxide positive electrodes," *J. Power Sources*, vol. 278, pp. 473–483, Mar. 2015. [Online]. Available: <https://www.sciencedirect.com/science/article/pii/S0378775314020758>
- [115] M. Mauri, F. Castelli-Dezza, M. S. Carmeli, M. Scarfogliero, and G. Marchegiani, "Electro-thermal aging model of Li-ion batteries for vehicle-to-grid services," in *Proc. AEIT Int. Conf. Electr. Electron. Technol. Automot. (AEIT AUTOMOTIVE)*, Jul. 2019, pp. 1–6.
- [116] A. Hoke, A. Brissette, K. Smith, A. Pratt, and D. Maksimovic, "Accounting for lithium-ion battery degradation in electric vehicle charging optimization," *IEEE J. Emerg. Sel. Topics Power Electron.*, vol. 2, no. 3, pp. 691–700, Sep. 2014.
- [117] K. Smith, M. Earleywine, E. Wood, J. Neubauer, and A. Pesaran, (Jun. 1, 2012). *Comparison of Plug-in Hybrid Electric Vehicle Battery Life Across Geographies and Drive-Cycles*. [Online]. Available: <https://www.osti.gov/biblio/1044471>

- [118] L. Su *et al.*, "Identifying main factors of capacity fading in lithium ion cells using orthogonal design of experiments," *Appl. Energy*, vol. 163, pp. 201–210, Feb. 2016. [Online]. Available: <https://www.sciencedirect.com/science/article/pii/S0306261915014555>
- [119] V. Sangwan, R. Kumar, and A. K. Rathore, "An empirical capacity degradation modeling and prognostics of remaining useful life of Li-ion battery using unscented Kalman filter," in *Proc. 8th IEEE India Int. Conf. Power Electron. (IICPE)*, Dec. 2018, pp. 1–6.
- [120] H. Dai, X. Zhang, W. Gu, X. Wei, and Z. Sun, "A semi-empirical capacity degradation model of EV Li-ion batteries based on Eyring equation," in *Proc. IEEE Vehicle Power Propuls. Conf. (VPPC)*, Oct. 2013, pp. 1–5.
- [121] Y. Gao, J. Jiang, C. Zhang, W. Zhang, Z. Ma, and Y. Jiang, "Lithium-ion battery aging mechanisms and life model under different charging stresses," *J. Power Sources*, vol. 356, pp. 103–114, Jul. 2017. [Online]. Available: <https://www.sciencedirect.com/science/article/pii/S0378775317305876>
- [122] Y. Cui *et al.*, "Multi-stress factor model for cycle lifetime prediction of lithium ion batteries with shallow-depth discharge," *J. Power Sources*, vol. 279, pp. 123–132, Apr. 2015. [Online]. Available: <https://www.sciencedirect.com/science/article/pii/S037877531500004X>
- [123] J. Guo, Z. Li, and M. Pecht, "A Bayesian approach for Li-ion battery capacity fade modeling and cycles to failure prognostics," *J. Power Sources*, vol. 281, pp. 173–184, May 2015. [Online]. Available: <https://www.sciencedirect.com/science/article/pii/S0378775315001925>
- [124] S. S. Choi and H. S. Lim, "Factors that affect cycle-life and possible degradation mechanisms of a Li-ion cell based on LiCoO₂," *J. Power Sources*, vol. 111, no. 1, pp. 130–136, Sep. 2002. [Online]. Available: <https://www.sciencedirect.com/science/article/pii/S0378775302003051>
- [125] B. V. Ratnakumar, M. C. Smart, L. D. Whitenack, and R. C. Ewell, "The impedance characteristics of Mars exploration rover Li-ion batteries," *J. Power Sources*, vol. 159, no. 2, pp. 1428–1439, Sep. 2006.
- [126] C. Huang, J. Sakamoto, J. Wolfenstine, and S. Surampudi, "The limits of low-temperature performance of Li-ion cells," *J. Electrochem. Soc.*, vol. 147, no. 8, pp. 2893–2896, Aug. 2000.
- [127] S. Zhang, K. Xu, and R. Jow, "060. The low temperature performance of Li-ion batteries," *J. Power Sources*, vol. 115, pp. 137–140, Mar. 2003.
- [128] T. Waldmann, M. Wilka, M. Kasper, M. Fleischhammer, and M. Wohlfahrt-Mehrens, "Temperature dependent ageing mechanisms in lithium-ion batteries—A post-mortem study," *J. Power Sources*, vol. 262, pp. 129–135, Sep. 2014. [Online]. Available: <https://www.sciencedirect.com/science/article/pii/S0378775314004352>
- [129] M. Bauer, C. Guenther, M. Kasper, M. Petzl, and M. A. Danzer, "Discrimination of degradation processes in lithium-ion cells based on the sensitivity of aging indicators towards capacity loss," *J. Power Sources*, vol. 283, pp. 494–504, Jun. 2015. [Online]. Available: <https://www.sciencedirect.com/science/article/pii/S0378775315003766>
- [130] H.-P. Lin *et al.*, "Low-temperature behavior of Li-ion cells," *Electrochim. Solid-State Lett.*, vol. 4, no. 6, p. A71, 2001, doi: [10.1149/1.1368736](https://doi.org/10.1149/1.1368736).
- [131] G. Ning, B. Haran, and B. N. Popov, "Capacity fade study of lithium-ion batteries cycled at high discharge rates," *J. Power Sources*, vol. 117, nos. 1–2, pp. 160–169, 2003. [Online]. Available: <https://www.sciencedirect.com/science/article/pii/S0378775303000296>
- [132] S. S. Zhang, "The effect of the charging protocol on the cycle life of a Li-ion battery," *J. Power Sources*, vol. 161, no. 2, pp. 1385–1391, Oct. 2006. [Online]. Available: <https://www.sciencedirect.com/science/article/pii/S037877530611839>
- [133] K. Jalkanen, J. Karppinen, L. Skogström, T. Laurila, M. Nisula, and K. Vuorilehto, "Cycle aging of commercial NMC/graphite pouch cells at different temperatures," *Appl. Energy*, vol. 154, pp. 160–172, Sep. 2015. [Online]. Available: <https://www.sciencedirect.com/science/article/pii/S0306261915005735>
- [134] S. F. Schuster *et al.*, "Nonlinear aging characteristics of lithium-ion cells under different operational conditions," *J. Energy Storage*, vol. 1, pp. 44–53, Jun. 2015. [Online]. Available: <https://www.sciencedirect.com/science/article/pii/S2352152X15000092>
- [135] P. Niehoff, E. Kraemer, and M. Winter, "Parametrisation of the influence of different cycling conditions on the capacity fade and the internal resistance increase for lithium nickel manganese cobalt oxide/graphite cells," *J. Electroanal. Chem.*, vol. 707, pp. 110–116, Oct. 2013. [Online]. Available: <https://www.sciencedirect.com/science/article/pii/S1572665713003925>
- [136] T. Borsche, A. Ulbig, M. Koller, and G. Andersson, "Power and energy capacity requirements of storages providing frequency control reserves," in *Proc. IEEE Power Energy Soc. Gen. Meeting*, Jul. 2013, pp. 1–5.
- [137] S. Ganterbein, M. Schönleber, M. Weiss, and E. Ivers-Tiffée, "Capacity fade in lithium-ion batteries and cyclic aging over various state-of-charge ranges," *Sustainability*, vol. 11, no. 23, p. 6697, Nov. 2019. [Online]. Available: <https://www.mdpi.com/2071-1050/11/23/6697>
- [138] M. P. Mercer *et al.*, "Transitions of lithium occupation in graphite: A physically informed model in the dilute lithium occupation limit supported by electrochemical and thermodynamic measurements," *Electrochim. Acta*, vol. 324, Nov. 2019, Art. no. 134774. [Online]. Available: <https://www.sciencedirect.com/science/article/pii/S0013468619316457>
- [139] M. Koller, T. Borsche, A. Ulbig, and G. Andersson, "Defining a degradation cost function for optimal control of a battery energy storage system," in *Proc. IEEE Grenoble Conf.*, Jun. 2013, pp. 1–6.
- [140] K.-Y. Oh *et al.*, "Rate dependence of swelling in lithium-ion cells," *J. Power Sources*, vol. 267, pp. 197–202, Dec. 2014. [Online]. Available: <https://www.sciencedirect.com/science/article/pii/S0378775314007228>
- [141] J. Dahn, "Phase diagram of Li_xC₆," *Phys. Rev. B, Condens. Matter*, vol. 44, no. 17, pp. 9170–9177, 1991. [Online]. Available: <https://www.scopus.com/inward/record.uri?eid=2-s2.0-0000846309&doi=10.1103%2fPhysRevB.44.9170&partnerID=40&md5=e777836b078d70d65c9ef02252f94a8b>
- [142] T. F. Fuller, M. Doyle, and J. Newman, "Simulation and optimization of the dual lithium ion insertion cell," *J. Electrochem. Soc.*, vol. 141, no. 1, pp. 1–10, Jan. 1994. [Online]. Available: <https://www.scopus.com/inward/record.uri?eid=2-s2.0-0028320402&doi=10.1149%2f21&partnerID=40&md5=20ed1c34676320d56974bbc245545c61>
- [143] W.-J. Zhang, "Structure and performance of LiFePO₄ cathode materials: A review," *J. Power Sources*, vol. 196, no. 6, pp. 2962–2970, Mar. 2011. [Online]. Available: <https://www.sciencedirect.com/science/article/pii/S037877531002104X>
- [144] C. Masquelier, S. Patoux, C. Wurm, and M. Morcrette, "Polyanion-based positive electrode materials," Laboratoire de Reactivite et Chime des Solides, Amiens, France, Tech. Rep., Jan. 2003.
- [145] X. Shu, Y. Guo, W. Yang, K. Wei, and G. Zhu, "Life-cycle assessment of the environmental impact of the batteries used in pure electric passenger cars," *Energy Rep.*, vol. 7, pp. 2302–2315, Nov. 2021. [Online]. Available: <https://www.sciencedirect.com/science/article/pii/S2352484721002547>
- [146] D. Deng, "Li-ion batteries: Basics, progress, and challenges," *Energy Sci. Eng.*, vol. 3, no. 5, pp. 385–418, Sep. 2015, doi: [10.1002/ese3.95](https://doi.org/10.1002/ese3.95).
- [147] V. Etacheri, R. Marom, R. Elazari, G. Salitra, and D. Aurbach, "Challenges in the development of advanced Li-ion batteries: A review," *Energy Environ. Sci.*, vol. 4, no. 9, pp. 3243–3262, Aug. 2011, doi: [10.1039/C1EE01598B](https://doi.org/10.1039/C1EE01598B).
- [148] E. Martinez-Laserna *et al.*, "Technical viability of battery second life: A study from the ageing perspective," *IEEE Trans. Ind. Appl.*, vol. 54, no. 3, pp. 2703–2713, May/Jun. 2018.
- [149] E. W. J. Neubauer, K. Smith, and A. Pesaran, "Identifying and overcoming critical barriers to widespread second use of PEV batteries," Nat. Renew. Energy Lab., Golden, CO, USA, Tech. Rep. NREL/TP-5400-63332, 2015. [Online]. Available: <https://www.nrel.gov/docs/fy15osti/63332.pdf>
- [150] I. Aghabali, J. Bauman, P. J. Kollmeyer, Y. Wang, B. Bilgin, and A. Emadi, "800-V electric vehicle powertrains: Review and analysis of benefits, challenges, and future trends," *IEEE Trans. Transport. Electricif.*, vol. 7, no. 3, pp. 927–948, Sep. 2021.
- [151] FASTNED. (2021). *Fastned Vehicles and Charging Tips*. [Online]. Available: <https://support.fastned.nl/hc/en-gb/sections/115000180588-Vehicles-charging-tips?page=1#articles>



Wiljan Vermeer (Student Member, IEEE) received the bachelor's degree in electrical engineering from the Eindhoven University of Technology, Eindhoven, The Netherlands, in 2016, and the master's degree in electrical engineering from the Delft University of Technology, Delft, The Netherlands, in 2018, where he is currently pursuing the Ph.D. degree in solar-powered smart charging systems.

His research interests include electric vehicle (EV) smart charging, battery degradation, and dc-dc power electronic converters for smart charging.



Gautham Ram Chandra Mouli (Member, IEEE) received the bachelor's degree in electrical engineering from the National Institute of Technology Trichy, Tiruchirappalli, India, in 2011, the master's degree in electrical engineering from the Delft University of Technology (TU Delft), Delft, The Netherlands, in 2013, and the Ph.D. degree from TU Delft in 2018 for the development of a solar-powered vehicle-to-grid (V2G) electric vehicle charger compatible with Charge de Move (CHAdeMO), Combined Charging System (CCS)/COMBO, and designed smart charging algorithms (with PRE, Breda, ABB, Rijswijk, and The University of Texas at Austin (UT Austin), Austin, TX, USA).

From 2017 to 2019, he was a Post-Doctoral Research with TU Delft pursuing his research on power converters for electric vehicle (EV) charging, smart charging of EVs, trolley buses. He is currently an Assistant Professor with the DC Systems, Energy Conversion and Storage Group, Department of Electrical Sustainable Energy, TU Delft. He is involved in many projects with industrial and academic partners at the national- and EU-level concerning electric mobility and renewable energy, such as photo-voltaic (PV) charging of electric vehicles, orchestrated smart charging in mass deployment (OSCD), Trolley 2.0, Flexgrid, Flexinet, and NEON. He is a Coordinator and a Lecturer for the Massive Open Online Course (MOOC) on Electric cars on edX.org with 175 000 learners from 175 countries. His current research focuses on electric vehicles and charging, PV systems, power electronics, and intelligent control.

Dr. Chandra Mouli's Ph.D. degree was awarded the "Most Significant Innovation in Electric Vehicles" Award from IDTechEx in 2018 and the "Best Tech Idea of 2018" by KJK. He was awarded the Best Paper Prize in the IEEE TRANSACTIONS ON INDUSTRIAL INFORMATICS in 2018, the Best Poster Prize at the Erasmus Energy Forum 2016, The Netherlands, and the Best Paper Prize at the IEEE INDICON Conference 2009, India. He is also the Vice-Chair of the IEEE Industrial Electronic Society Benelux Chapter.



Pavol Bauer (Senior Member, IEEE) received the master's degree in electrical engineering from the Technical University of Košice, Košice, Slovakia, in 1985, and the Ph.D. degree from the Delft University of Technology, Delft, The Netherlands, in 1995.

From 2002 to 2003, he was with KEMA (DNV GL), Arnhem, The Netherlands, on different projects related to power electronics applications in power systems. He is currently a Full Professor with the Department of Electrical Sustainable Energy, Delft University of Technology, where he is also the Head of the DC Systems, Energy Conversion and Storage Group. He is also a Professor with the Brno University of Technology, Brno, Czechia, and an Honorary Professor with Politehnica University Timișoara, Timișoara, Romania. He has worked on many projects for industry concerning wind and wave energy, power electronic applications for power systems, such as Smartrafo and HVdc systems, projects for smart cities, such as photo-voltaic (PV) charging of electric vehicles, PV and storage integration, and contactless charging, and participated in several Leonardo da Vinci, H2020, and Electric Mobility Europe EU projects as a Project Partner (ELINA, INETELE, E-Pragmatic, Micact, Trolley 2.0, orchestrated smart charging in mass deployment (OSCD), P2P, and Progressus) and a Coordinator (PEMCWebLab.com-Edipe, SustEner, and Eranet DCMICRO). He has authored or coauthored more than 120 journal articles and 500 conference papers in his field with an H factor Google scholar of 40 and Web of Science of 26. He is the author or a coauthor of eight books. He holds seven international patents and organized several tutorials at international conferences. His main research focuses on power electronics for charging electric vehicles and dc grids.

Dr. Bauer is also a member of the Executive Committee of the European Power Electronics Association and the International Steering Committee at numerous conferences. He is also the Former Chairperson of the Benelux IEEE Joint Industry Applications Society and the Power Electronics and Power Engineering Society Chapter and the Chairperson of the Power Electronics and Motion Control Council.